The Plant Cell, Vol. 17, 2020–2036, July 2005, www.plantcell.org

A Rab-E GTPase Mutant Acts Downstream of the Rab-D Subclass in Biosynthetic Membrane Traffic to the Plasma Membrane in Tobacco Leaf Epidermis [W]

Huanquan Zheng,[a,1] Luísa Camacho,[b] Edmund Wee,[a] Henri Batoko,[a,2] Julia Legen,[a] Christopher J. Leaver,[a] Rui Malhó,[c] Patrick J. Hussey,[b] and Ian Moore[a,3]

[a] Department of Plant Sciences, University of Oxford, Oxford, OX1 3RB, United Kingdom
[b] Integrative Cell Biology Laboratory, School of Biological and Biomedical Sciences, University of Durham, Durham, DH1 3LE, United Kingdom
[c] Universidade de Lisboa, Faculdade de Ciências de Lisboa, Instituto de Ciencia Aplicada e Tecnologia, 1749-016 Lisboa, Portugal

The function of the Rab-E subclass of plant Rab GTPases in membrane traffic was investigated using a dominant-inhibitory mutant (RAB-E1^d[NI]) of *Arabidopsis thaliana* RAB-E1^d and in vivo imaging approaches that have been used to characterize similar mutants in the plant Rab-D2 and Rab-F2 subclasses. RAB-E1^d[NI] inhibited the transport of a secreted green fluorescent protein marker, secGFP, but in contrast with dominant-inhibitory RAB-D2 or RAB-F2 mutants, it did not affect the transport of Golgi or vacuolar markers. Quantitative imaging revealed that RAB-E1^d[NI] caused less intracellular secGFP accumulation than RAB-D2^a[NI], a dominant-inhibitory mutant of a member of the Arabidopsis Rab-D2 subclass. Furthermore, whereas RAB-D2^a[NI] caused secGFP to accumulate exclusively in the endoplasmic reticulum, RAB-E1^d[NI] caused secGFP to accumulate additionally in the Golgi apparatus and a prevacuolar compartment that could be labeled by FM4-64 and yellow fluorescent protein (YFP)–tagged Arabidopsis RAB-F2^b. Using the vacuolar protease inhibitor E64-d, it was shown that some secGFP was transported to the vacuole in control cells and in the presence of RAB-E1^d[NI]. Consistent with the hypothesis that secGFP carries a weak vacuolar-sorting determinant, it was shown that a secreted form of DsRed reaches the apoplast without appearing in the prevacuolar compartment. When fused to RAB-E1^d, YFP was targeted specifically to the Golgi via a saturable nucleotide- and prenylation-dependent mechanism but was never observed on the prevacuolar compartment. We propose that RAB-E1^d[NI] inhibits the secretory pathway at or after the Golgi, causing an accumulation of secGFP in the upstream compartments and an increase in the quantity of secGFP that enters the vacuolar pathway.

INTRODUCTION

The plant endomembrane system consists of several biochemically distinct membrane-bound organelles that are responsible for the biosynthesis of proteins, polysaccharides, and lipids. In addition to its role in the biogenesis of the cell wall, plasma membrane (PM), and vacuole, the endomembrane system contributes to the control of development and to responses to biotic and abiotic stresses (Surpin and Raikhel, 2004). To achieve these ends and to maintain its own organization, the endomembrane system must correctly deliver newly synthesized proteins, polysaccharides, and lipids to a variety of specific cellular subcompartments. Moreover, if each compartment on the transport pathway is to maintain its distinct molecular and functional identity, it must retain specific subsets of the molecules it receives, and all this takes place in the face of rapid bidirectional membrane flux. Much remains to be learned about the transport pathways on the secretory, vacuolar, and endocytic routes that connect the organelles of the plant endomembrane system. It is particularly important to identify the molecules that ensure correct targeting of transport vesicles at each step on these pathways.

Genetic analysis in *Saccharomyces cerevisiae* and analysis of dominant Rab GTPase mutants in mammalian cells has revealed that the Rab GTPase family is a key component of these mechanisms. Rab GTPases cycle between an inactive cytosolic GDP-bound form and an active GTP-bound form that associates with specific membranes to ensure vesicle targeting specificity by regulating the activity of tethering factors, cytoskeletal factors, and, probably indirectly, soluble *N*-ethylmaleimide–sensitive factor attachment protein receptor complexes (Segev, 2001; Zerial and McBride, 2001). They can also act as local organizers of membrane identity (Zerial and McBride, 2001).

The Rab GTPase family in any organism comprises several functionally distinct subclasses that are each responsible for specific vesicle transport and fusion events (Pereira-Leal and

[1] Current address: Department of Botany, University of British Columbia, 3529-6270 University Boulevard, Vancouver, BC, V6T 1Z4, Canada.
[2] Current address: Unit of Plant Biology, Institut des Sciences de la Vie, Université Catholique de Louvain, Croix du Sud 5-13, B-1348 Louvain-la-Neuve, Belgium.
[3] To whom correspondence should be addressed. E-mail ian.moore@plants.ox.ac.uk; fax 44-1865-275074.
The author responsible for distribution of materials integral to the findings presented in this article in accordance with the policy described in the Instructions for Authors (www.plantcell.org) is: Ian Moore (ian.moore@plants.ox.ac.uk).
[W] Online version contains Web-only data.
Article, publication date, and citation information can be found at www.plantcell.org/cgi/doi/10.1105/tpc.105.031112.

Seabra, 2000, 2001; Segev, 2001; Zerial and McBride, 2001). Regions outside four conserved nucleotide binding motifs differ between Rab subclasses and account for functional specialization by interacting with subclass-specific factors and by targeting proteins to specific membrane domains (Moore et al., 1995; Pereira-Leal and Seabra, 2000; Segev, 2001; Zerial and McBride, 2001). The *Arabidopsis thaliana* genome sequence contains 57 loci that encode putative Rab GTPases, substantially greater than the number in yeast but similar to the number of known Rab sequences in humans (Arabidopsis Genome Initiative, 2000; Pereira-Leal and Seabra, 2001; Rutherford and Moore, 2002). Despite the similarity in the overall number of Rab GTPases in Arabidopsis and humans, it is striking that most of the 40 or so mammalian Rab subclasses are absent from plant genomes (Pereira-Leal and Seabra, 2001; Rutherford and Moore, 2002). These differences may reflect the specific membrane trafficking events that occur in each organism (Pereira-Leal and Seabra, 2000, 2001; Rutherford and Moore, 2002). It remains unclear, however, how many distinct functional Rab subclasses are present in higher plants. In phylograms, all angiosperm Rab GTPase sequences fall into just eight clades, Rab-A to Rab-H, which are clearly related to specific Rab subclasses in yeasts and/or mammals (Pereira-Leal and Seabra, 2001; Rutherford and Moore, 2002; Vernoud et al., 2003). However, considering the large number and diversity of Rab sequences within many of these clades, it has been suggested that functional specialization may have taken place within clades during angiosperm evolution and that 18 or so functional subclasses may exist (Pereira-Leal and Seabra, 2001; Rutherford and Moore, 2002; Vernoud et al., 2003). Further clarification will require functional data from plant cells, but this is very limited. Dominant-negative mutants have been used to investigate the roles of members of the Rab-B, Rab-D2, and Rab-F2 subclasses in particular cell types (Batoko et al., 2000; Cheung et al., 2002; Sohn et al., 2003; Bolte et al., 2004; Kotzer et al., 2004), but functional data is entirely lacking for five of the eight major clades and for 14 of the 18 putative subclasses.

In this study, we examined the function of the plant Rab-E subclass. This is the nearest neighbor of the Rab-D clade that we have shown to be involved in endoplasmic reticulum (ER)–Golgi traffic (Batoko et al., 2000; Saint-Jore et al., 2002). The Rab-E subclass is related to Sec4p of *S. cerevisiae*, to Ypt2 of *Schizosaccharomyces pombe*, and to mammalian Rab8, Rab10, and Rab13 as well as several other paralogous mammalian Rab subclasses that have no orthologs in plants or yeasts (Pereira-Leal and Seabra, 2001; Rutherford and Moore, 2002). Sec4p, Ypt2, and the mammalian subclasses that are most similar to the plant Rab-E subclass have demonstrated or implied roles in Golgi–PM traffic or exocytosis (Segev, 2001).

The Rab-E subclass in Arabidopsis has five members, RAB-E1^{a} to RAB-E1^{e}, two of which appear to have arisen through major chromosomal duplication events (Rutherford and Moore, 2002). Members of the Arabidopsis Rab-E subclass are rapidly upregulated in response to ethylene, suggesting a role for them in the ethylene response (Moshkov et al., 2003). In tomato (*Lycopersicon esculentum*), mRNA for a Rab-E protein (Tm3) has been shown to localize to the flanks and the uppermost cell layers of the shoot apical meristem (Fleming et al., 1993), and two Rab-E proteins (Api2 and Api3) have been identified as interactors and potential targets of the *Pseudomonas syringae* AvrPto protein (Bogdanove and Martin, 2000). It has been proposed that AvrPto may inhibit vesicle traffic to the PM of the infected cells perhaps by interfering with Rab-E function (Bogdanove and Martin, 2000; Hauck et al., 2003). A role for RAB-E1^{a} in *Agrobacterium tumefaciens*–mediated transformation has also been proposed (Hwang and Gelvin, 2004). However, there is no evidence relating to the intracellular trafficking function of the Rab-E subclass in plants.

In this study, we analyzed the cellular function of the plant Rab-E GTPase subclass using a transient trafficking assay that has been used to characterize Arabidopsis RAB-D2^{a} (ARA5/AtRab1b), RAB-F2^{b} (ARA7), SAR1, and tobacco (*Nicotiana tabacum*) Syp121 (Nt-Syr1) in tobacco epidermal cells (Batoko et al., 2000; Geelen et al., 2002; Saint-Jore et al., 2002; daSilva et al., 2004; Kotzer et al., 2004). We provide evidence that a dominant-inhibitory mutant of Arabidopsis RAB-E1^{d} functions differently from the equivalent mutant of RAB-D2^{a} and inhibits trafficking from the Golgi apparatus to the PM.

RESULTS

A Dominant-Inhibitory Mutant in RAB-E1^{d} Results in Increased Intracellular Secreted Green Fluorescent Protein Accumulation

To investigate the trafficking functions of the plant Rab-E subclass, we generated a dominant-negative mutant allele of one member of the Arabidopsis Rab-E subclass, RAB-E1^{d} (At5g03520). This mutant, RAB-E1^{d}[NI], carries a single amino acid substitution, Asn128 to Ile, in the conserved GTP binding motif GNKxD. The corresponding substitution in many Rab and other Ras-like GTPases reduces affinity for nucleotide, resulting in dominant-negative alleles that have provided valuable information on the trafficking functions of the respective Rab proteins in yeasts, mammals, and plants (Schmitt et al., 1986; Walworth et al., 1989; Bourne et al., 1991; Bucci et al., 1992; Walch-Solimena et al., 1997; Batoko et al., 2000; Segev, 2001; Zerial and McBride, 2001; Cheung et al., 2002; Rutherford and Moore, 2002). The corresponding mutation in the yeast ortholog of Rab-E1^{d}, Sec4[N133I], has been extensively characterized and shown to be a specific dominant inhibitor of Sec4 function in transport from the Golgi to PM and to interact with the nucleotide exchange factor Sec2 (Walworth et al., 1989; Walch-Solimena et al., 1997).

The effect of RAB-E1^{d}[NI] on biosynthetic membrane traffic was analyzed in a transport assay previously used to characterize dominant mutants of Arabidopsis RAB-D2^{a} (ARA5; AtRab1b; At1g02130, a member of the Rab-D2 subclass), RAB-F2^{b} (ARA7; At4g19640), SAR1, and a tobacco syntaxin (Batoko et al., 2000; Geelen et al., 2002; Saint-Jore et al., 2002; daSilva et al., 2004; Kotzer et al., 2004). This assay is based on a secreted green fluorescent protein marker, secGFP, which is transported from the ER to the apoplast where it accumulates poorly and exhibits weak fluorescence (Boevink et al., 1999; Batoko et al., 2000; Zheng et al., 2004). Under conditions that inhibit biosynthetic traffic to the apoplast, fluorescent secGFP protein

accumulates inside the cells and can be readily visualized in the endomembrane compartments (Batoko et al., 2000). Both the wild-type and mutant cDNAs of RAB-E1^{d} were coexpressed with secGFP by Agrobacterium-mediated transfection of tobacco lower epidermal cells as described previously (Batoko et al., 2000). Sixty-five to 72 h after infiltration, secGFP fluorescence intensity was examined by confocal laser scanning microscopy at low magnification. At this time, control cells expressing only secGFP exhibited very dim fluorescence (Figures 1A and 1B) in comparison with cells expressing an ER-resident GFP marker, GFP-HDEL (Figures 1A and 1C). Coexpression of secGFP with a dominant-inhibitory allele of Arabidopsis RAB-D2^{a}, RAB-D2^{a}[NI], that has been shown to inhibit transport between the ER and Golgi apparatus (Batoko et al., 2000), resulted in an increase in GFP fluorescence owing to intracellular accumulation of secGFP (Figure 1D). When secGFP was coexpressed with wild-type RAB-E1^{d} (Figure 1E), the fluorescence appeared to be unaltered relative to secGFP alone (Figure 1B), suggesting that wild-type RAB-E1^{d} did not affect biosynthetic traffic of secGFP under these conditions. By contrast, in the presence of RAB-E1^{d}[NI], a significant increase in GFP fluorescence and intracellular accumulation was detected (Figure 1F). Quantitative analysis of confocal images confirmed that tissues cotransfected with RAB-E1^{d}[NI] had approximately five times the fluorescence intensity of tissues coexpressing RAB-E1^{d} but approximately half the intensity measured in the presence of RAB-D2^{a}[NI] (Figure 1G). These data suggest that RAB-E1^{d}[NI] inhibited secGFP traffic but less efficiently than RAB-D2^{a}[NI].

In the Presence of RAB-E1^{d}[NI], secGFP Labels ER and Post-ER Punctate Structures

To establish whether or not RAB-E1^{d}[NI] caused secGFP to accumulate in the same compartments as RAB-D2^{a}[NI], we examined tissues expressing each mutant at higher resolution by confocal laser scanning microscopy. In most epidermal cells of leaf tissues infiltrated with secGFP alone, secGFP fluorescence was barely detectable, but in a few cells secGFP was seen either in the apoplast (Figure 2A), in a network interpreted as ER by comparison to GFP-HDEL (Figure 2B), or in unidentified mobile punctate structures in addition to the ER. In the presence of RAB-D2^{a}[NI], however, intracellular secGFP appeared to have accumulated exclusively in the ER network (Figure 2C, inset), as reported previously (Batoko et al., 2000). By contrast, in cells that accumulated most secGFP in the presence of RAB-E1^{d}[NI], GFP was observed in numerous small mobile punctate structures of unknown identity in addition to the ER network (Figure 2D, inset and arrowheads). Control cells expressing secGFP alone occasionally accumulated fluorescent GFP in the ER and in similar punctate structures. Therefore, to determine the effect of RAB-E1^{d}[NI] and RAB-D2^{a}[NI] mutants more precisely, we counted the number of visibly fluorescent cells per field of view in tissues infiltrated with secGFP alone or with secGFP plus either RAB-E1^{d}[NI] or RAB-D2^{a}[NI] and determined the subcellular distribution of secGFP in each fluorescent cell with a 40×/1.2 numerical aperture (NA) objective lens. As shown in Figure 2E, the presence of RAB-E1^{d}[NI] increased the number of fluorescent cells and the

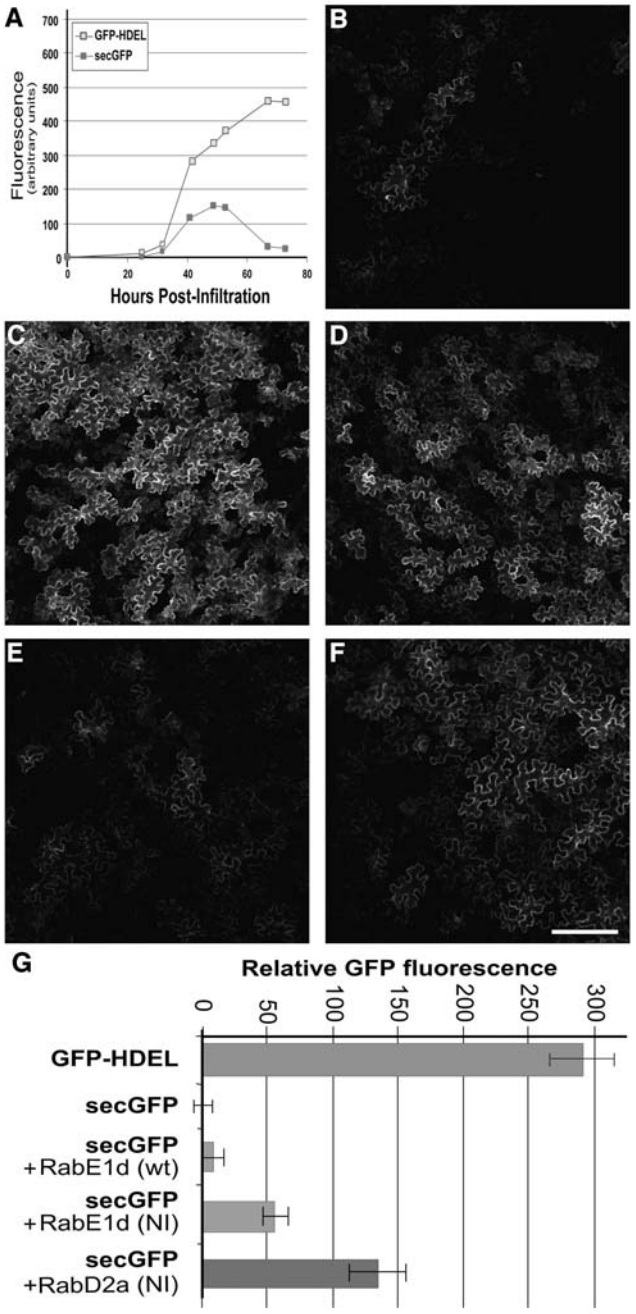

Figure 1. A Dominant-Inhibitory Mutant in RAB-E1^{d} Results in Increased Intracellular secGFP Accumulation.

(A) Time course of GFP-HDEL and secGFP fluorescence during transient expression in tobacco leaf epidermal cells infected with the respective Agrobacterium strains.

(B) to **(F)** Confocal images at low magnification of tobacco leaf epidermal cells expressing secGFP **(B)**, GFP-HDEL **(C)**, secGFP+RAB-D2^{a}[NI] **(D)**, secGFP+RAB-E1^{d} **(E)**, and secGFP+RAB-E1^{d}[NI] **(F)**. Bar in **(F)** = 100 μm for **(B)** to **(F)**.

(G) Relative GFP fluorescence intensity of tobacco leaf epidermal cells expressing GFP-HDEL, secGFP, secGFP + RAB-E1^{d}, secGFP + RAB-E1^{d}[NI], and secGFP + RAB-D2^{a}[NI].

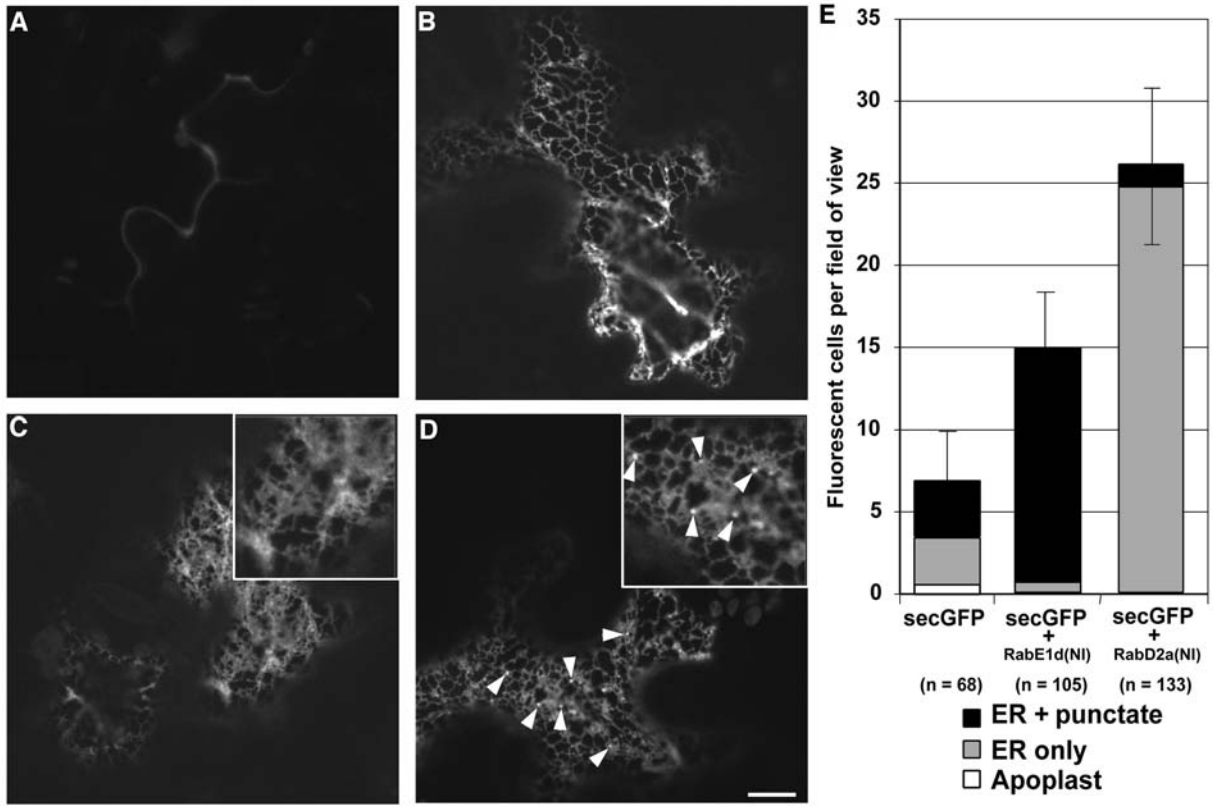

Figure 2. secGFP Labels ER and Post-ER Punctate Structures in the Presence of RAB-E1^{d}[NI].

(A) to **(D)** Confocal images at high magnification of tobacco leaf epidermal cells expressing secGFP **(A)**, GFP-HDEL **(B)**, secGFP + RAB-D2^{a}[NI] **(C)**, and secGFP + RAB-E1^{d}[NI] **(D)**. Note the punctate structures indicated by arrowheads in the image **(D)** and the inset. Bar in **(D)** = 10 μm for **(A)** to **(D)**.
(E) Average number of fluorescent cells and frequency of particular intracellular fluorescence patterns per field of view in cells expressing secGFP, secGFP + RAB-E1^{d}[NI], and secGFP + RAB-D2^{a}[NI]. n is the number of cells scored.

proportion of cells that accumulated GFP in punctate structures as well as in the ER. By contrast, expression of RAB-D2^{a}[NI] resulted in a pronounced reduction in the percentage of cells that exhibited GFP fluorescence in punctate structures despite a marked increase in the total number of fluorescent cells. These results confirmed that RAB-E1^{d}[NI] resulted in a mild but significant increase in intracellular secGFP accumulation and indicated that RAB-E1^{d}[NI] and RAB-D2^{a}[NI] had opposite effects on the accumulation of secGFP in the small punctate structures.

Expression of RAB-E1^{d}[NI] Affects Vesicle Trafficking Downstream of the Golgi Apparatus

To investigate the identity of the small punctate structures that accumulated secGFP in the presence of RAB-E1^{d}[NI], we first asked whether they represented either a domain of the ER or a sorting compartment between the ER and Golgi. To do this, we examined cells that accumulated secGFP after cotransfecting leaf tissues with secGFP, RAB-E1^{d}[NI], and the ER marker yellow fluorescent protein (YFP)-HDEL (Brandizzi et al., 2002a) constructs. YFP-HDEL contains a C-terminal HDEL tetrapeptide that promotes receptor-mediated retrieval to the ER (Denecke et al., 1992; Crofts et al., 1999), so if the punctate structures that accumulate secGFP in the presence of RAB-E1^{d}[NI] are part of the ER or the retrieval pathway, they should also accumulate YFP-HDEL. We found that YFP-HDEL colocalized with secGFP in the ER network but did not mark the small punctate secGFP structures (Figures 3A to 3D, arrows; see Supplemental Movies 1 and 2 online), indicating that these structures were distinct from the ER and were unlikely to represent an intermediate on the ER retrieval pathway. To test whether the secGFP-labeled punctate structures represented an ER–Golgi intermediate that was incompatible with YFP fluorescence, the ER markers YFP-HDEL and GFP-HDEL were coexpressed with RAB-E1^{d}[NI], and in all cells examined YFP and GFP fully colocalized (e.g., Figure 3E). This confirmed that GFP-HDEL does not label a compartment that is incompatible with YFP fluorescence and further suggested that the punctate structures that are labeled by secGFP were not derived from the ER retrieval pathway.

Coexpression of YFP-HDEL with secGFP and RAB-E1^{d}[NI] highlighted the existence of a second type of punctate structure that was faintly labeled by secGFP in the presence of RAB-E1^{d}[NI] (Figures 3C and 3D, arrowheads). As with the

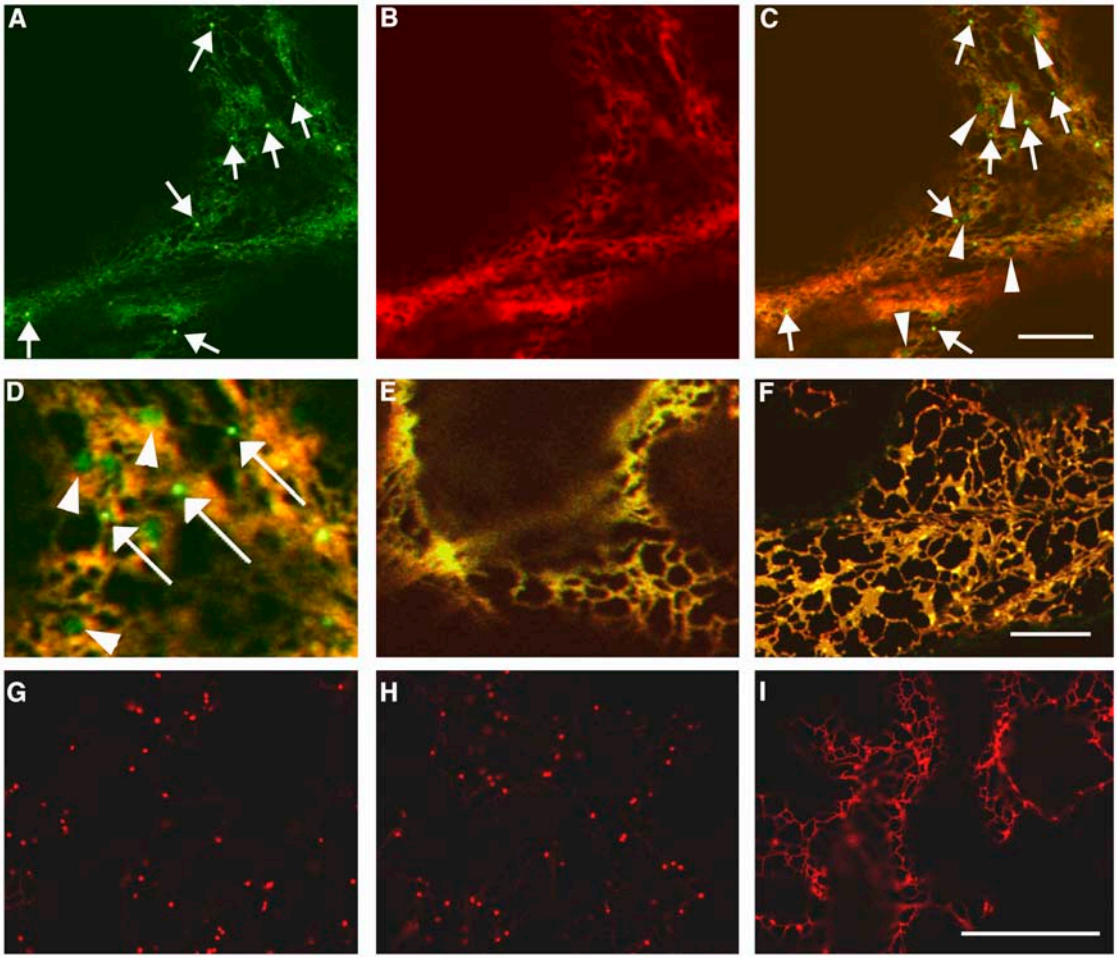

Figure 3. Expression of RAB-E1^{d}[NI] Does Not Directly Affect ER-to-Golgi Trafficking.

(A) to **(C)** Confocal images of a tobacco epidermal cell expressing secGFP **(A)** and YFP-HDEL **(B)** in presence of RAB-E1^{d}[NI]. **(C)** was obtained by merging images **(A)** and **(B)**. Note that the punctate compartments labeled by secGFP fluorescence (arrows) are not marked by YFP-HDEL fluorescence. Note also the existence of a second type of punctate structure that is faintly labeled by secGFP but excludes YFP-HDEL (arrowheads in **[C]**). Bar in **(C)** = 10 μm for **(A)** to **(C)**.

(D) Enlarged image of the confocal image in **(C)** showing details of small but bright (arrows) and apparently larger but faint (arrowheads) punctate structures labeled by secGFP but not by YFP-HDEL in the presence of RAB-E1^{d}[NI].

(E) and **(F)** Merged GFP/YFP confocal images of tobacco leaf epidermal cells expressing GFP-HDEL + YFP-HDEL in the presence of RAB-E1^{d}[NI] **(E)** and secGFP + YFP-HDEL in the presence of RAB-D2^{a}[NI] **(F)**. Bar in **(F)** = 5 μm for **(D)** to **(F)**.

(G) to **(I)** Confocal images of tobacco leaf epidermal cells expressing ST-YFP **(G)**, ST-YFP + RAB-E1^{d}[NI] **(H)**, and ST-YFP + RAB-D2^{a}[NI] **(I)**. Bar in **(I)** = 10 μm for **(G)** to **(I)**.

small punctate structures initially observed, these structures excluded YFP-HDEL (Figures 3C and 3D, arrowheads), indicating they were also post-ER compartments and were mobile (see Supplemental Movies 1 and 2 online). However, they were apparently larger and exhibited dimmer fluorescence than the other punctate structures. In contrast with the complex distribution of secGFP in the presence of RAB-E1^{d}[NI], when secGFP was coexpressed with RAB-D2^{a}[NI], it accumulated exclusively in the reticular network where it colocalized precisely with YFP-HDEL (Figure 3F), consistent with the previous conclusion that RAB-D2^{a}[NI] inhibits membrane traffic between the ER and Golgi apparatus (Batoko et al., 2000). These observations suggested that RAB-E1^{d}[NI] behaves differently from RAB-D2^{a}[NI] on biosynthetic membrane traffic, acting downstream of the ER and probably not upstream of the ER retrieval compartment.

One possible explanation for the accumulation of secGFP in the ER and post-ER compartments in the presence of RAB-E1^{d}[NI] is that RAB-E1^{d}[NI] might act directly in both ER–Golgi traffic and in a subsequent trafficking step. Alternatively, RAB-E1^{d}[NI] might act specifically at a later stage of biosynthetic traffic causing secGFP to accumulate initially in post-ER compartments, with accumulation upstream arising as a secondary effect. To test if RAB-E1^{d}[NI] directly inhibits ER–Golgi membrane trafficking, we next examined whether it inhibited

Golgi targeting of sialyltransferase (ST)-YFP, a YFP-based Golgi marker (Brandizzi et al., 2002b). Consistent with previous observations (Batoko et al., 2000; Saint-Jore et al., 2002), when ST-YFP was coexpressed with RAB-D2^{a}[NI], ST-YFP redistributed from a punctate pattern typical of the Golgi apparatus to the ER, though residual labeling of Golgi stacks was still evident (Figure 3I). By contrast, coexpression of ST-YFP with RAB-E1^{d}[NI] had little if any effect on the localization of the Golgi marker (Figure 3H). Moreover the YFP-labeled Golgi stacks were similar in apparent size and number to those of control cells (Figure 3G). These observations provided further evidence that RAB-E1^{d}[NI] and RAB-D2^{a}[NI] have distinct effects on biosynthetic membrane traffic and suggested that, unlike RAB-D2^{a}, RAB-E1^{d}[NI] might not act directly in ER–Golgi transport.

In the Presence of RAB-E1^{d}[NI], secGFP Accumulates in the Golgi Stacks and in a Prevacuolar Compartment

To identify the post-ER punctate structures that accumulated secGFP in the presence of RAB-E1^{d}[NI], a variety of endomembrane markers were coexpressed with secGFP and RAB-E1^{d}[NI]. Because the larger, fainter punctate structures that accumulated secGFP in the presence of RAB-E1^{d}[NI] were reminiscent of Golgi stacks with respect to their number, motility, and morphology in the confocal microscope (Boevink et al., 1998), secGFP was coexpressed with RAB-E1^{d}[NI] and the Golgi marker ST-YFP (Brandizzi et al., 2002b). Because the larger secGFP-labeled punctate structures were often slightly brighter than the associated ER network, they could be identified by careful examination even in the absence of YFP-HDEL (Figures 4A, 4D, arrowheads, and 8A, red arrows). Strikingly, ST-YFP colocalized with these large, faint punctate structures (Figures 4A to 4F, arrowheads) but not with the smaller brighter ones (Figures 4A to 4F, arrows; a second example is given in Supplemental Figure 1A online). When control cells coexpressing ST-YFP without secGFP were imaged with identical imaging parameters, there was no visible signal in the GFP image (Figures 4G to 4I), excluding the possibility that the Golgi-sized faint punctate structures represented bleed-through of YFP fluorescence into the GFP detection channel.

The small punctate structures that accumulated secGFP in the presence of RAB-E1^{d}[NI] were amongst those structures labeled by FM4-64 (Figures 4J to 4L, white arrows; see also Supplemental Figure 1B for other examples and Supplemental Movie 3 online), a dye that can label a variety of vacuolar, prevacuolar, and endosomal or putatively endosomal compartments in a variety of plant cells (Ueda et al., 2001, 2004; Geldner et al., 2003; Bolte et al., 2004). To further clarify the identity of the small punctate structures, we performed a double labeling experiment with YFP-RAB-F2^{b} (Kotzer et al., 2004). RAB-F2^{b} (ARA7) is involved in the sorting of proteins with sequence-specific vacuolar sorting signals, and tagged RAB-F2^{b} is known to localize predominantly to a prevacuolar compartment (PVC) that can be labeled by FM4-64, by markers derived from plant vacuolar sorting receptors, and by soluble vacuole-targeted markers (Ueda et al., 2001; Sohn et al., 2003; Kotzer et al., 2004; Lee et al., 2004). When secGFP was coexpressed with YFP-RAB-F2^{b} and RAB-E1^{d}[NI], the small, bright punctate structures labeled by secGFP (Figures 4M and 4O, arrows) were also marked by YFP-RAB-F2^{b} (Figure 4N, arrows), indicating that these structures represent a PVC (see Supplemental Figure 1C and Movie 4 online).

RAB-E1^{d}[NI] Does Not Alter the Distribution of a Vacuole-Targeted Marker

Because expression of RAB-E1^{d}[NI] caused secGFP to accumulate in both Golgi and PVCs, it raised the question whether RAB-E1^{d}[NI] inhibited only the biosynthetic pathway to the PM or also vacuolar traffic. To clarify this, we tested the effect of RAB-E1^{d}[NI] on the vacuolar transport of spo:GFP (Sohn et al., 2003), a GFP variant that travels from the ER to the central lytic vacuole via the Golgi apparatus and a PVC (Sohn et al., 2003). When spo:GFP was expressed alone in tobacco epidermal cells, GFP fluorescence was dim but could be seen in punctate structures (Figure 5A) that represent a PVC (Takeuchi et al., 2000; Sohn et al., 2003). Fluorescence was not observed in the central vacuole, suggesting that spo:GFP may not be sufficiently stable or fluorescent in this compartment under our growth conditions (Tamura et al., 2003). As expected, cells that were cotransfected with spo:GFP and RAB-D2^{a}[NI] exhibited markedly increased GFP fluorescence in a reticulate network typical of the ER (cf. Figures 5A and 5C), consistent with the view that spo:GFP is normally transported rapidly from the ER via the Golgi apparatus to the vacuole where it fails to accumulate. By contrast, coexpression with RAB-E1^{d}[NI] did not alter spo:GFP fluorescence intensity or distribution, and the GFP-labeled PVC compartments were similar in apparent size and number to those of control cells (Figure 5B). Moreover, we did not observe extracellular accumulation of spo:GFP in the presence of RAB-E1^{d}[NI] as reported when dominant-negative Rab-F2^{a} or Rab-F2^{b} mutants were coexpressed with vacuolar GFP markers in Arabidopsis protoplasts or tobacco leaves (Sohn et al., 2003; Kotzer et al., 2004). Thus, RAB-E1^{d}[NI] appears not to affect spo:GFP transport to the vacuole along the ER-Golgi-PVC pathway. These observations are also consistent with the previous conclusion that RAB-E1^{d}[NI] does not act directly in ER-to-Golgi transport and suggest rather that RAB-E1^{d}[NI] acts specifically in the late secretory pathway to the apoplast.

secGFP Is Transported to the Vacuole in the Presence of RAB-E1^{d}[NI]

The presence of secGFP in a YFP-RAB-F2^{b}-positive PVC in some control cells (Figure 2E) suggested that at least a portion of the secGFP protein enters the vacuolar pathway. The increased labeling of the PVC in the presence of RAB-E1^{d}[NI] (Figure 2E) could be explained if the Rab mutant inhibits secGFP trafficking between the Golgi and apoplast resulting in more secGFP entering the vacuolar pathway. Alternatively, RAB-E1^{d}[NI] may act at the PVC to inhibit secGFP traffic from PVC to vacuole or PM. To investigate these possibilities, we first asked whether secGFP indeed traffics to the vacuole in the absence and presence of RAB-E1^{d}[NI].

If a proportion of secGFP is transported to the vacuole from the PVC, its presence there may be difficult to determine owing to the large volume, low pH, and proteolytic activity of this

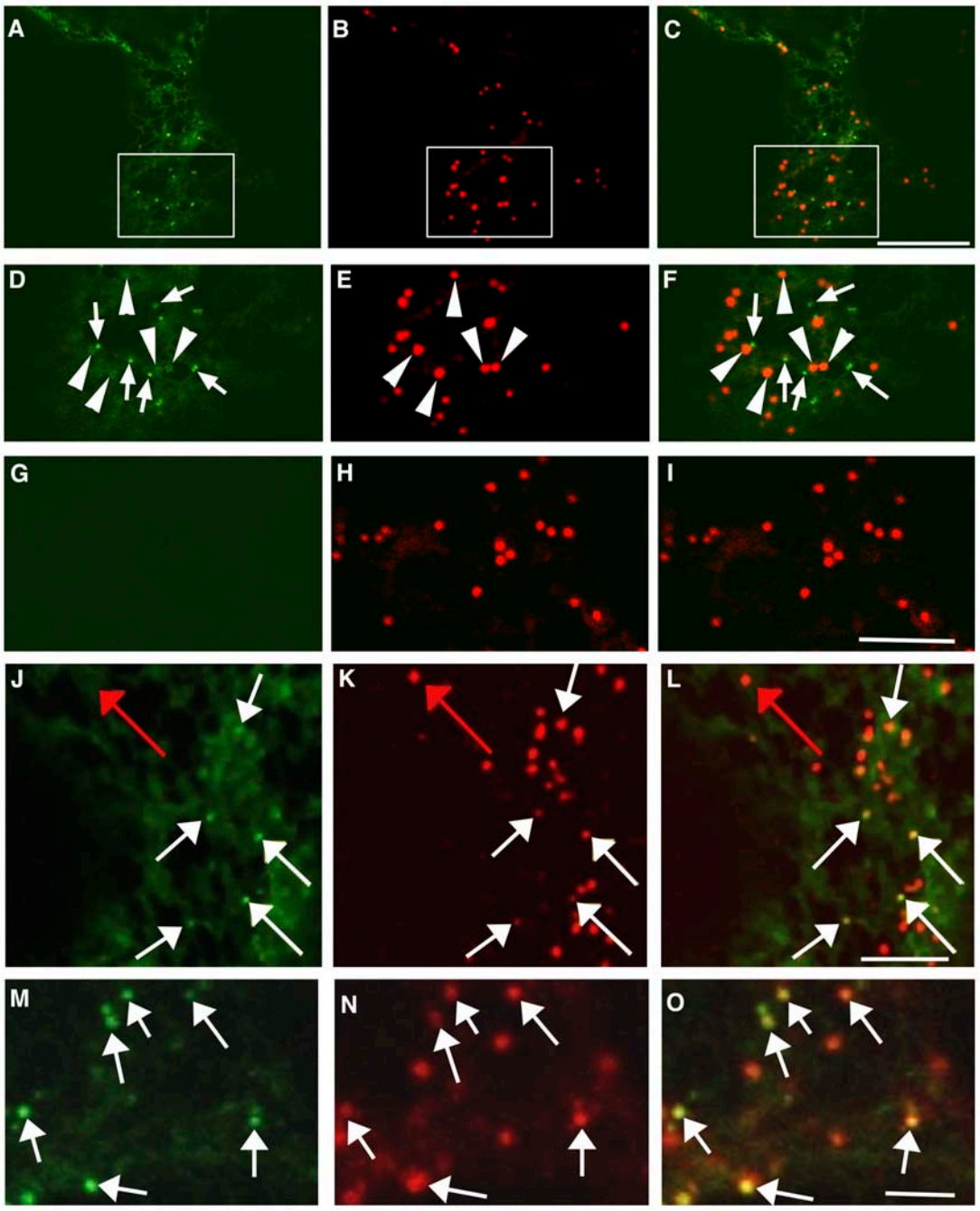

Figure 4. In the Presence of RAB-E1^{d}[NI], secGFP Accumulates in the Golgi Stacks and in a PVC.

(A) to **(F)** Confocal images of a tobacco epidermal cell expressing secGFP (**[A]** and **[D]**) and ST-YFP (**[B]** and **[E]**) in the presence of RAB-E1^{d}[NI]. **(C)** is a merge of **(A)** and **(B)**. **(D)** to **(F)** are enlarged images of **(A)** to **(C)**, respectively. Note the colocalization of ST-YFP fluorescence with the large, faint secGFP punctate structures (arrowheads in **[D]** to **[F]**). The small, bright secGFP punctate structures (arrows image **[D]** and **[F]**) do not colocalize with ST-YFP. Bar in **(C)** = 10 μm for **(A)** to **(C)**.

(G) to **(I)** Confocal images of a control tobacco epidermal cell coexpressing ST-YFP and RAB-E1^{d}[NI] without secGFP. Imaging parameters were identical to those used for **(A)** to **(F)**. No signal is visible in the GFP image **(G)** excluding the possibility that the Golgi-sized faint punctate structures represent bleed-through of YFP fluorescence into the GFP detection channel in **(A)** and **(D)**. Bar in **(I)** = 5 μm for **(D)** to **(I)**.

(J) to **(L)** Confocal images of an FM4-64–stained tobacco leaf epidermal cell from a region coinfiltrated with secGFP and RAB-E1^{d}[NI]. **(L)** is a merged image from the secGFP image **(J)** and the FM4-64 image **(K)**. White arrows identify examples of small brightly labeled secGFP punctate structures marked by FM4-64 **(K)**. Red arrow indicates a structure apparently labeled by FM4-64 alone. Bar in **(L)** = 2 μm for **(J)** to **(L)**.

(M) to **(O)** Confocal images of a tobacco leaf epidermal cell coexpressing secGFP and YFP-RAB-F2^{b} in the presence of RAB-E1^{d}[NI]. **(O)** was obtained by merging the secGFP image **(M)** and YFP-RAB-F2^{b} image **(N)**. Arrows indicate examples of small brightly labeled secGFP punctate structures that are labeled by YFP-RAB-F2^{b} fluorescence **(N)**. Bar in **(O)** = 1 μm for **(M)** to **(O)**.

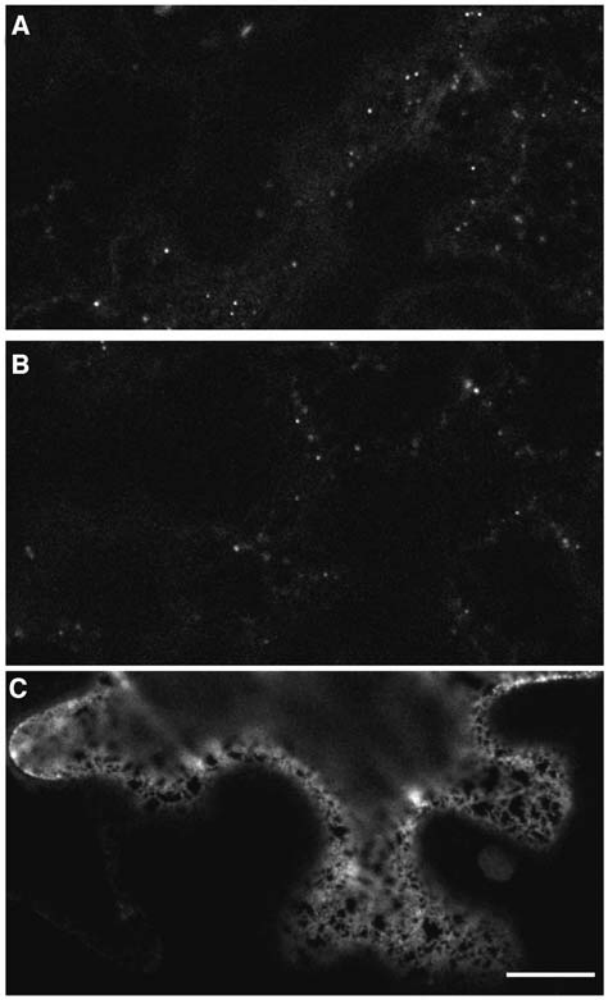

Figure 5. RAB-E1^{d}[NI] Does Not Alter the Distribution of the Vacuole-Targeted Marker spo:GFP.

Confocal images of tobacco epidermal cells expressing spo:GFP **(A)**, spo:GFP + RAB-E1^{d}[NI] **(B)**, and spo:GFP + RAB-D2^{a}[NI] **(C)**. Bar in **(C)** = 10 μm for **(A)** to **(C)**.

compartment. It has been reported that GFP can be stabilized in the vacuoles of Arabidopsis and tobacco cells by treatment with the membrane-permeant protease inhibitor E64-d, particularly in the dark (Tamura et al., 2003, 2004). Therefore, we investigated the accumulation of secGFP and GFP-HDEL in E64-d–treated tissues. In these experiments, infiltration was performed with Agrobacterium harboring pVKH-secGFP at OD_{600} 0.03 (three times the usual titre) to ensure high rates of secGFP synthesis and transport. Thirty six hours after infiltration with Agrobacterium, shortly after the onset of secGFP accumulation (see Figure 1A), transfected areas of the leaf were infiltrated with E64-d, then excised from the plant and floated on a solution of E64-d in darkness for 14 h. Confocal imaging revealed that secGFP was clearly detectable in the vacuoles of infected epidermal cells, whereas GFP-HDEL was largely excluded (see Supplemental Figure 2 online).

We used the same method to investigate the effect of RAB-E1^{d}[NI] and RAB-D2^{a}[NI] on the transport and accumulation of secGFP in tissues treated with E64-d. All confocal images were acquired with the same imaging parameters, which were chosen to allow detection of the vacuolar signals in the control samples without excessive saturation of signal from the RAB-D2^{a}[NI] sample. Coexpression of RAB-E1^{d}[NI] did not inhibit secGFP accumulation in the vacuole but rather enhanced it (Figure 6C) relative to controls expressing RAB-E1^{d} (Figure 6B) or secGFP alone (Figure 6A), whereas RAB-D2^{a}[NI] prevented secGFP from reaching the vacuole (Figure 6D). Consistent with these findings, quantitative estimates of secGFP accumulation in the vacuole indicated a twofold increase in the presence of RAB-E1^{d}[NI] relative to controls expressing wild-type RAB-E1^{d} or secGFP alone (data not shown).

To further investigate transport to the vacuole in the presence of RAB-E1^{d}[NI], we used E64-d to investigate vacuolar accumulation of aleu-GFP. This is a GFP derivative that carries a vacuolar sorting signal from *Petunia hybrida* aleurain (Humair et al., 2001) and that has recently been shown to reach the vacuole via a RAB-F2^{b}–dependent pathway in tobacco epidermal cells (Kotzer et al., 2004). Using conditions described by Kotzer et al. (2004), aleu-GFP was expressed in tobacco epidermal cells either alone or with RAB-E1^{d}, RAB-E1^{d}[NI], RAB-D2^{a}[NI], or a dominant-negative RAB-F2^{b} mutant (RAB-F2^{b}[SN]). Thirty-three to 36 h after infiltration, infected areas of leaf tissue were treated with E64-d in darkness, and 12 to 14 h later confocal images were collected. Imaging parameters were chosen to allow detection of the vacuolar signals in the control samples without excessive saturation of signal from the RAB-D2^{a}[NI] and RAB-F2^{b}[SN] samples. In control cells (Figures 6E to 6H), aleu-GFP was visible in the vacuoles and punctate PVCs as well as in the apoplast of some cells (arrowheads), owing most probably to saturation of the vacuolar sorting receptors under these conditions (apoplastic fluorescence was particularly noticeable in some infiltrations; see for example Supplemental Figure 3 online). In the presence of RAB-E1^{d}[NI], vacuolar and prevacuolar fluorescence of aleu-GFP was still clear (Figures 6I and 6J), and peripheral staining in the apoplast was significantly reduced (arrowheads; see Supplemental Figure 3 online). By contrast, accumulation of aleu-GFP in the vacuole was inhibited by RAB-F2^{b}[SN] and RAB-D2^{a}[NI] (Figures 6K and 6M). RAB-F2^{b}[SN] caused a dramatic increase in aleu-GFP fluorescence in the apoplast and in punctate structures (Figure 6L), as described previously (Kotzer et al., 2004), whereas RAB-D2^{a}[NI] caused aleu-GFP to accumulate in the ER (Figure 6N) in accordance with our observations with the vacuolar marker spo:GFP (Figures 5A and 5C). Examining samples at higher magnification confirmed that RAB-E1^{d}[NI] did not cause aleu-GFP to accumulate in the ER (data not shown), consistent with our previous observations with spo:GFP (Figure 5B). The marked differences in the distribution of aleu-GFP caused by dominant-negative mutants of the Rab-E, Rab-D2, and Rab-F2 subclasses provide further evidence of the distinct and specific action of each class of mutant in tobacco epidermal cells.

These observations confirmed that (1) a proportion of the secGFP molecules can be transported to the vacuole (at least when steady state rates of synthesis are high), (2) RAB-E1^{d}[NI] does not inhibit transport of secGFP or aleu-GFP to the vacuole,

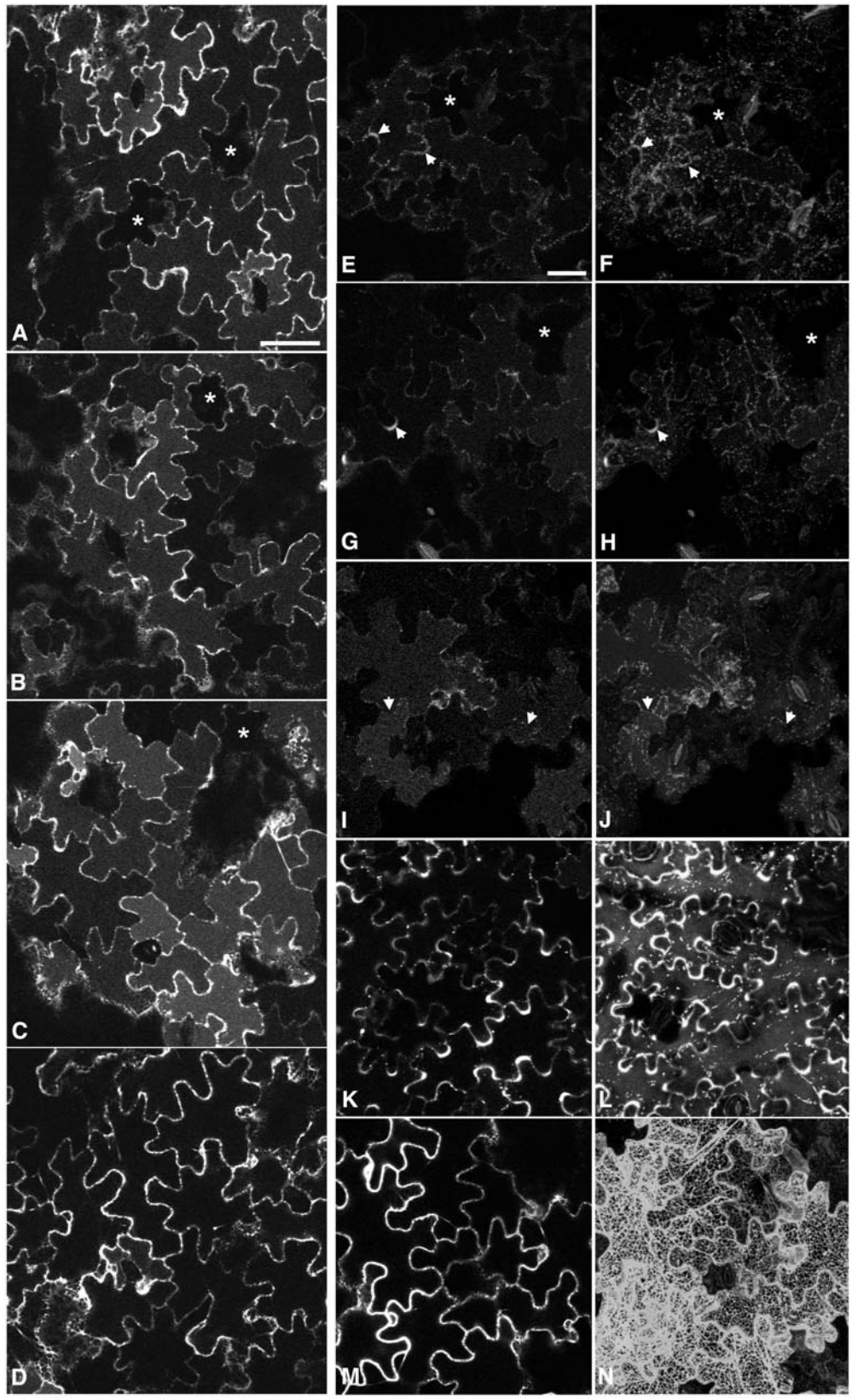

Figure 6. secGFP and aleu-GFP Are Transported to the Vacuole in the Presence and Absence of RAB-E1^{d}[NI].

and (3) RAB-E1^d[NI] appears to increase the proportion of secGFP that accumulates in the vacuole relative to the cell wall. Thus, the accumulation of secGFP in PVC in the presence of RAB-E1^d[NI] could reflect an increase in the proportion of secGFP that enters the Golgi-to-vacuole pathway. However, we also considered the possibility that the PVC may lie on the pathway between Golgi and apoplast and that RAB-E1^d[NI] may act at or beyond this compartment to inhibit the transport of secGFP to the apoplast. To test these possibilities, we investigated the membrane targeting specificity of RAB-E1^d and asked whether the PVC lies on the default pathway to the apoplast.

RAB-E1^d Targets YFP to the Golgi but Not the PVC

Because Rab proteins must be targeted to specific compartments to perform their function, we asked whether RAB-E1^d carried information for targeting heterologous proteins to either the Golgi or PVC. YFP was fused to the N terminus of wild-type RAB-E1^d, RAB-E1^d[SN] (a mutant carrying the S29N substitution that is predicted to restrict the protein to the GDP-bound form), and RAB-E1^{d}ΔCC, which lacks the conserved Cys residues that are required for C-terminal prenylation and membrane attachment (Seabra and Wasmeier, 2004). The resulting fusions were coexpressed in tobacco epidermal cells with the Golgi marker ST-GFP (Boevink et al., 1998). As shown in Figure 7, YFP-RAB-E1^d was exclusively localized to the cytoplasm and punctate structures (Figure 7A) positive for ST-GFP (Figures 7B and 7C), indicating that RAB-E1^d has specific targeting information for Golgi stacks. Labeling of the Golgi was most evident in cells that exhibited the lowest expression levels, becoming increasingly difficult to distinguish from the cytosolic pool as YFP-RAB-E1^d expression levels increased (data not shown). This suggests that Golgi labeling was a saturable process. Moreover, the two mutant alleles, YFP-RAB-E1^d[SN] (Figure 7D) and YFP-RAB-E1^{d}ΔCC (Figure 7G), were exclusively cytosolic, strongly suggesting that RAB-E1^d requires both normal nucleotide binding and C-terminal prenylation to target YFP to the Golgi apparatus.

In contrast with the precise colocalization of YFP-RAB-E1^d to the Golgi apparatus, YFP-tagged RAB-D2^a labeled Golgi-associated punctate structures that were also observed in complete isolation from Golgi stacks (Figures 7J to 7L, arrows). Again, targeting was dependent on normal GTP binding as the YFP-RAB-D2^a[S22N] mutant was cytosolic (Figure 7M).

To examine if there was any fraction of RAB-E1^d associated with the secGFP-labeled PVC compartment, we coexpressed secGFP and YFP-RAB-E1^d. In cells where intracellular secGFP could be identified in small bright (Figure 8A, inset and white arrows) and large faint (Figure 8A, inset and red arrows) punctate structures, YFP-RAB-E1^d colocalized to the latter (red arrows) but not to the former (white arrows) (Figures 8A to 8C, insets), indicating that RAB-E1^d did not associate with the PVC and confirming its location on Golgi stacks (see Supplemental Movie 5 online). Images of cells expressing YFP-RAB-E1^d in the absence of intracellular secGFP (Figures 8D to 8F) excluded the possibility that the weak GFP signal in the large punctate structures in Figure 8A was bleed-through from YFP-RAB-E1^d to the GFP channel. These observations indicate that RAB-E1^d has the capacity to target YFP specifically to the Golgi apparatus and suggest that this organelle is its likely site of action.

The Default Pathway to the Apoplast Does Not Involve the RAB-F2^b-Positive PVC

Finally, we investigated why secGFP was detected in the RAB-F2^b-positive PVC. Although secGFP has previously been observed in, and isolated from, the apoplast (Boevink et al., 1999; Batoko et al., 2000; Zheng et al., 2004), it is nevertheless possible that it carries a cryptic vacuolar sorting determinant that promotes the entry of some proportion of the secGFP into the vacuolar pathway. Alternatively, it may be that the default pathway to the apoplast includes the RAB-F2^b-positive PVC from which vacuolar and secreted proteins are sorted. If the PVC does lie on the default pathway, it should be labeled by other secreted proteins. To test this hypothesis, we constructed a secreted form of monomeric red fluorescent protein1 (mRFP1), a monomeric derivative of DsRed (Campbell et al., 2002) that is unrelated to GFP and foreign to plants. This marker, secRFP, was coexpressed with secGFP in tobacco epidermal cells, which were imaged ~50 h after infiltration when the rate of marker expression and transport was at its highest (Figure 1A). In cells with the highest steady state levels of secGFP and secRFP transport, both proteins were visible in the ER, but the PVC was labeled by secGFP only (Figures 9A and 9C, insets and arrows). Nevertheless, secRFP was clearly observed in the apoplast, where it was stable and accumulated in a fluorescent form (Figures 9B and 9C). This demonstrates that not all secreted

Figure 6. (continued).

Agrobacterium harboring pVKH-secGFP was infiltrated into tobacco leaves at OD_{600} 0.03 (three times the usual titre), and the aleu-GFP strain was infiltrated at OD_{600} 0.1 as described previously (Kotzer et al., 2004). All samples were treated with E64-d in darkness for 12 to 14 h and were imaged ~50 h after inoculation with Agrobacterium. Asterisks identify cells that express little or no GFP and indicate the background vacuolar fluorescence in these images. Bars = 50 μm.

(A) to **(D)** Medial confocal sections through abaxial epidermal cells indicating secGFP fluorescence in E64-d–treated leaves. **(A)** secGFP only; **(B)** secGFP coinfiltrated with RAB-E1^d; **(C)** secGFP coinfiltrated with RAB-E1^d[NI]; **(D)** secGFP coinfiltrated with RAB-D2^a[NI].

(E) to **(N)** Location of aleu-GFP in the presence of dominant-inhibitory Rab GTPase mutants in single optical sections (**[E]**, **[G]**, **[I]**, **[K]**, and **[M]**) through abaxial epidermal cells and in projections (**[F]**, **[H]**, **[J]**, **[L]**, and **[N]**) of series of optical sections on the *z* axis through the outer cortical region of abaxial epidermal cells. **(E)** and **(F)** aleu-GFP alone; **(G)** and **(H)** aleu-GFP + RAB-E1^d; **(I)** and **(J)** aleu-GFP + RAB-E1^d[NI]; **(K)** and **(L)** aleu-GFP + RAB-F2^b[SN]; **(M)** and **(N)** aleu-GFP + RAB-D2^a[NI]. Arrows indicate regions of apoplast between infected cells that exhibit clear aleu-GFP fluorescence in **(E)** to **(H)** but are weakly fluorescent in **(I)** and **(J)**.

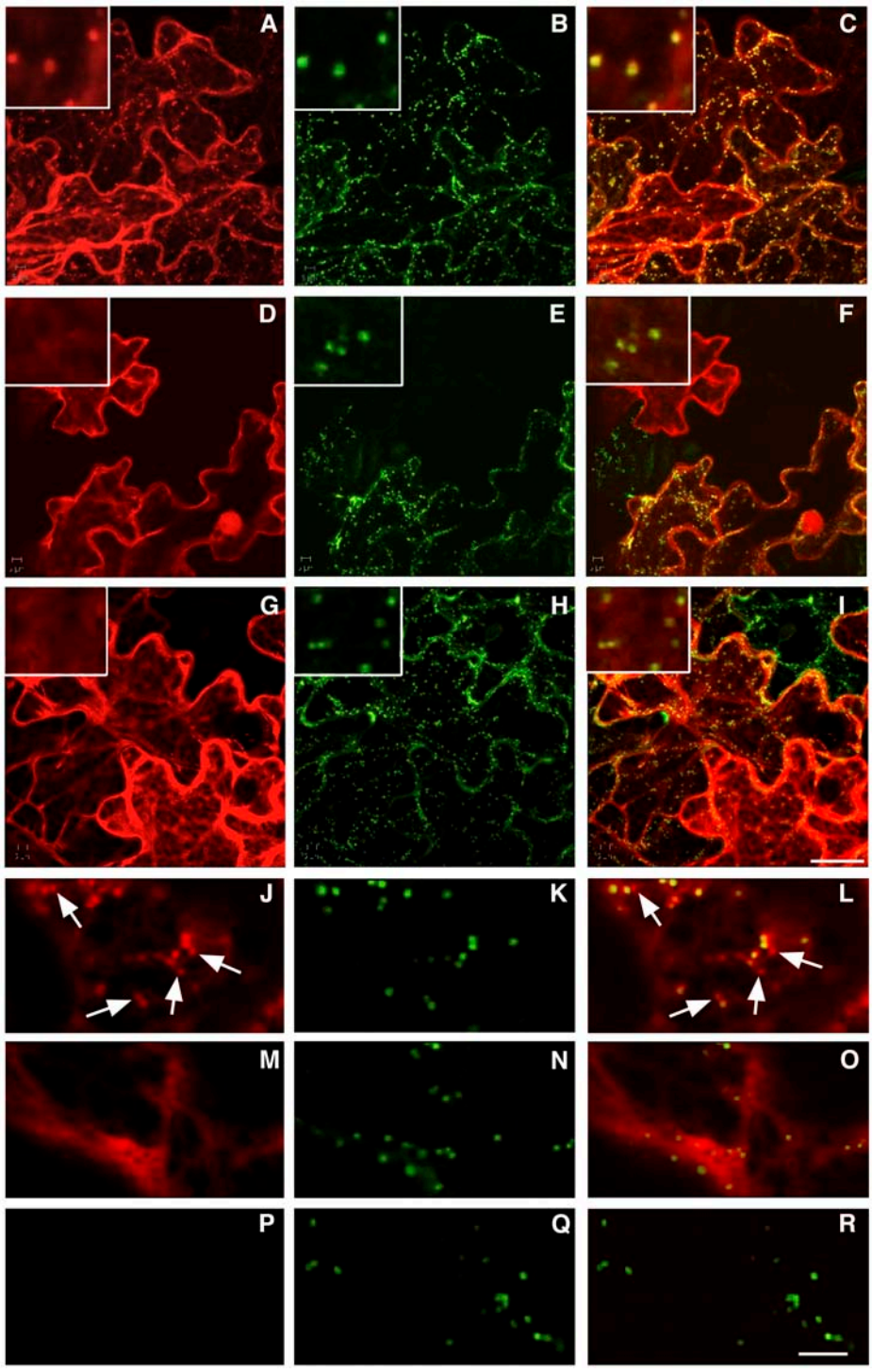

Figure 7. RAB-E1^{d} Targets YFP to the Golgi via a GTP- and Prenylation-Dependent Mechanism.

(A) to **(C)** Confocal analysis of cells coexpressing YFP-RAB-E1^{d} **(A)** and ST-GFP **(B)**. **(C)** is merged from the YFP-RAB-E1^{d} image **(A)** and the ST-GFP image **(B)**. Note the precise colocalization of YFP-RAB-E1^{d}–labeled punctate structures and Golgi (insets).

(D) to **(F)** Confocal analysis of tobacco epidermal cells coexpressing YFP-RAB-E1^{d}[SN] **(D)** and ST-GFP **(E)**. **(F)** was obtained by merging images **(D)** and **(E)**. Note the exclusively cytosolic YFP-RAB-E1^{d}[SN] fluorescence in **(D)**.

(A) to **(I)** are projections on the *z* axis of a series of optical sections of the cortical cytoplasm. Bar in **(I)** = 25 μm for **(A)** to **(I)**.

(G) to **(I)** Confocal analysis of tobacco epidermal cells coexpressing YFP-RAB-E1^{d}ΔCC **(G)** and ST-GFP **(H)**. **(I)** was obtained by merging **(G)** and **(H)**.

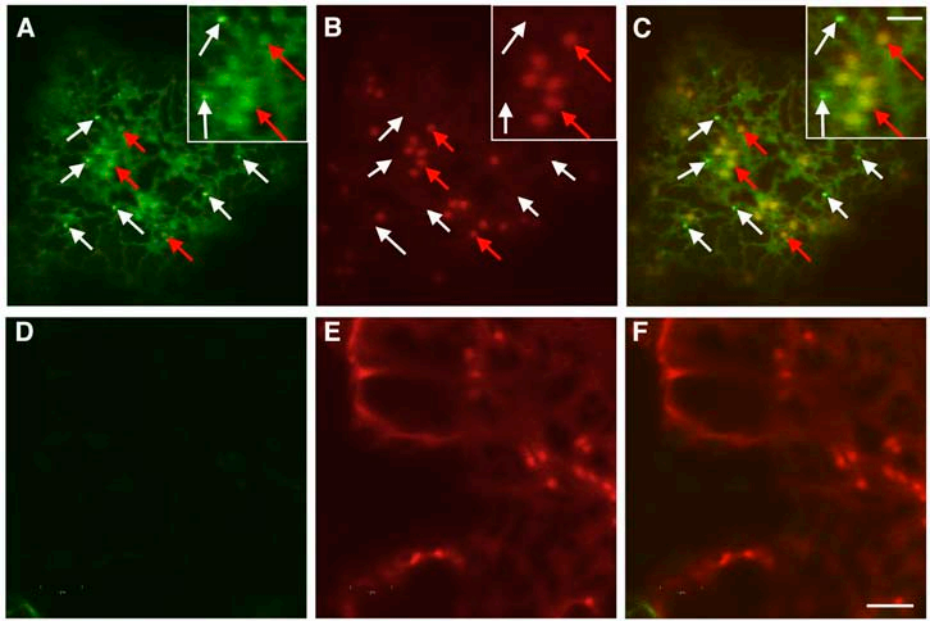

Figure 8. YFP-Tagged RAB-E1^{d} Does Not Label the PVC That Accumulates secGFP.

(A) to **(C)** Confocal images of a tobacco epidermal cell coexpressing secGFP and YFP-RAB-E1^{d} at ~50 h after infiltration, when secGFP accumulation is highest (Figure 1A). **(C)** is the merged image of secGFP fluorescence **(A)** and YFP-RAB-E1^{d} fluorescence **(B)**. White arrows in **(A)** to **(C)** and insets indicate examples of small, bright punctate structures that are labeled by secGFP but not by YFP-RAB-E1^{d}. Red arrows indicate examples of large, faint Golgi punctate structures that are labeled by YFP-RAB-E1^{d} fluorescence.

(D) to **(F)** Confocal images of a control tobacco epidermal cell expressing YFP-RAB-E1^{d} without secGFP. The images were captured with identical image settings used for **(A)** to **(C)**. **(F)** is merged from **(D)** and the YFP-RAB-E1^{d} image **(E)**. The absence of signal in the GFP image **(D)** excludes the possibility that the Golgi-sized faint punctate structures represent bleed-through of YFP fluorescence into the GFP detection channel. Bar in **(F)** = 5 μm for **(A)** to **(F)**; bar in inset **(C)** = 2 μm for all insets.

proteins accumulate in the PVC en route to the apoplast and argues in favor of a cryptic vacuolar sorting signal within secGFP that diverts a portion of the protein to the RAB-F2^{b}-positive PVC.

DISCUSSION

In this study, we investigated the function of RAB-E1^{d} in membrane traffic in the secretory pathway by expressing various fluorescent-tagged trafficking markers in the presence of the dominant-inhibitory RAB-E1^{d}[NI] allele in tobacco epidermal cells. In contrast with RAB-D2^{a}[NI], which inhibits ER-to-Golgi traffic (Batoko et al., 2000) causing secGFP to accumulate exclusively in the ER, we found that in the presence of RAB-E1^{d}[NI], secGFP accumulated in the Golgi, the ER, and a PVC, indicating that RAB-E1^{d}[NI] and RAB-D2^{a}[NI] had different effects on the transport of secGFP. Moreover, unlike RAB-D2^{a}[NI], RAB-E1^{d}[NI] did not affect either Golgi targeting of ST-YFP or ER-to-Golgi transport of vacuolar spo:GFP or aleu-GFP. Based on these observations, we propose that RAB-E1^{d}[NI] does not directly inhibit ER-to-Golgi trafficking but acts at or after the Golgi apparatus. This is further supported by the fact that RAB-E1^{d} can target YFP specifically to the Golgi stacks via a saturable GTP- and prenylation-dependent mechanism. We suggest that secGFP accumulates in the ER as a secondary consequence

Figure 7. (continued).

Like YFP-RAB-E1^{d}[SN], YFP-RAB-E1^{d}ΔCC fluorescence is exclusively cytosolic **(G)**. Insets in **(D)** to **(I)** show regions of each image at higher resolution, confirming that YFP-tagged RAB-E1^{d} mutants do not colocalize with Golgi stacks.

(J) to **(L)** Confocal analysis of a tobacco epidermal cell coexpressing YFP-RAB-D2^{a} **(J)** and ST-GFP **(K)**. **(L)** was obtained by merging **(J)** and **(K)**. Arrows identify examples of YFP-RAB-D2^{a}–labeled punctate structures that are distinct from the Golgi stacks.

(M) to **(O)** Confocal analysis of a tobacco epidermal cell coexpressing YFP-RAB-D2^{a}[SN] **(M)** and ST-GFP **(N)**. **(O)** was obtained by merging **(M)** and **(N)**. Note the exclusive cytosolic YFP-RAB-D2^{a}[SN] fluorescence in **(M)**.

(P) to **(R)** Confocal images of a control tobacco epidermal cell expressing ST-GFP. The images were captured with identical confocal laser scanning parameters used for **(J)** to **(O)**. **(R)** is merged from **(P)** and the ST-GFP image **(Q)**. The absence of signal in the YFP image **(P)** excludes the possibility that the Golgi-sized faint punctate structures in **(J)** represented bleed-through of GFP fluorescence into the YFP detection channel. Bar in **(R)** = 5 μm for **(J)** to **(R)**.

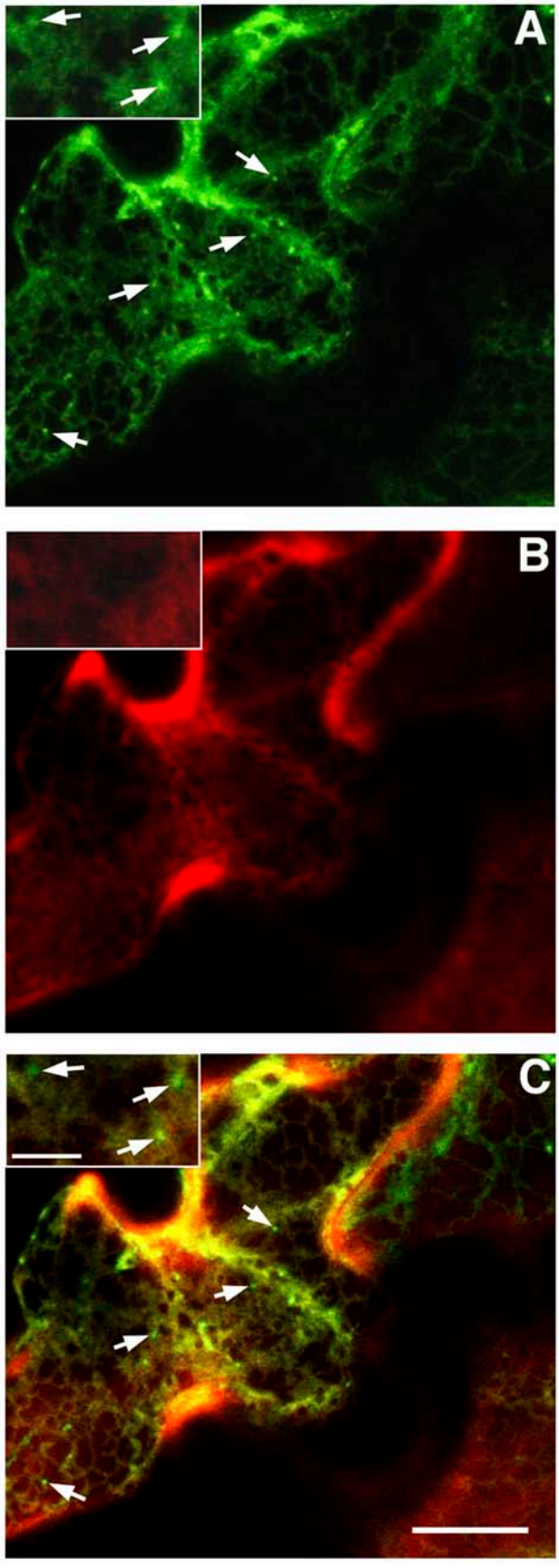

of RAB-E1^{d}[NI] action at the Golgi apparatus. A similar secondary effect on ER-to-Golgi transport of secGFP was postulated when membrane traffic was inhibited with a dominant-inhibitory peptide derived from a syntaxin (Geelen et al., 2002) that resides at the PM (Leyman et al., 2000). A disadvantage of all trafficking assays based on transient expression of dominant-inhibitory proteins is that the protein accumulates to inhibitory levels over a period of hours, whereas trafficking of the marker takes place over much shorter time scales (Phillips et al., 1988; Thiel et al., 1998; Brandizzi et al., 2002b). This makes it difficult to distinguish primary from secondary effects on membrane traffic, and it will take the development of conditional mutants and assays for initial trafficking rates to overcome this limitation in plant cells. In their absence, we presume that a particular mutant is most likely to act at or downstream of the latest compartment on the pathway that accumulates the marker. Thus, RAB-E1^{d}[NI] appears to act in post-Golgi traffic, and because it did not prevent vacuolar sorting of spo:GFP or aleu-GFP but enhanced the vacuolar accumulation of secGFP, we propose that RAB-E1^{d}[NI] acts in the Golgi-PM pathway. It is likely that inhibition of secGFP traffic from the Golgi to the PM by RAB-E1^{d}[NI] causes secGFP to accumulate in *trans*-Golgi compartments, and we suggest that this increases the quantity of secGFP that is diverted into the vacuolar pathway. This interpretation can account for the low overall accumulation of secGFP in the presence of RAB-E1^{d}[NI] (compared with the action of RAB-D2^{a}[NI]) and the increased labeling of RAB-F2^{b}-positive PVC and vacuoles by secGFP. Similar arguments can account for the observation that coexpression of aleu-GFP with Rab-E1^{d}[NI] in the presence of the vacuolar protease inhibitor E64-d resulted in a slight increase in vacuolar fluorescence and reduced apoplastic fluorescence relative to controls (Figures 6E, 6G, and 6I). This most probably reflects the secretion of a proportion of the aleu-GFP from control cells under these conditions owing to the saturable nature of vacuolar sorting via sequence-specific vacuolar sorting receptors (Paris and Neuhaus, 2002; Kotzer et al., 2004). We postulate that coexpression with RAB-E1^{d}[NI] reduces the loss of aleu-GFP via the Golgi-PM pathway while leaving the Golgi-vacuolar pathway functional.

In yeast, evidence has accumulated that at least two parallel routes mediate post-Golgi transport to the cell surface, one of which involves transport via a PVC/endosomal compartment and requires Pep12p (Harsay and Bretscher, 1995; Gurunathan et al., 2002; Harsay and Schekman, 2002). Each pathway employs distinct secretory vesicles and carries different cargoes, but Sec4p, the yeast Rab most similar to the plant Rab-E group, is required for both (Harsay and Bretscher, 1995; Gurunathan

Figure 9. The Default Pathway to the Apoplast Does Not Involve the RAB-F2^{b}-Positive PVC.

Confocal analysis of tobacco epidermal cells coexpressing secGFP **(A)** and secRFP **(B)**. **(C)** was obtained by merging **(A)** and **(B)**. Both secGFP **(A)** and secRFP **(B)** can be visualized in the ER, but the PVC labeled by secGFP (arrows in **[A]**, **[C]**, and insets) is exclusive of secRFP (arrows in **[C]** and insets). secRFP was clearly observed in the apoplast where it was stable **(B)**. Bar in **(C)** = 10 μm for **(A)** to **(C)**; bar in inset **(C)** = 3 μm for all insets.

et al., 2002; Harsay and Schekman, 2002). The route via the endosome is thought to be a specialized pathway that operates in addition to the direct default route to the PM, allowing cells to rapidly adjust the levels of selected molecules at the cell surface (Harsay and Schekman, 2002). Although we are not aware of any direct evidence for a similar route from Golgi via PVC to PM in plants, we cannot exclude the possibility that some secGFP reaches the apoplast from the PVC, in which case RAB-E1^{d}[NI] may additionally inhibit transport from the PVC to the apoplast in a manner similar to Sec4p (Gurunathan et al., 2002; Harsay and Schekman, 2002). However, our demonstration that secGFP can accumulate in E64-d–treated vacuoles and that YFP-RAB-E1^{d} labels the Golgi but not the PVC supports the simpler hypothesis that a cryptic vacuolar sorting determinant within GFP causes a proportion of the protein to be transported from the Golgi to the vacuole via a PVC. This view is consistent with the observation that secRFP does not label the PVC en route to the apoplast and also with the known requirement for a signal to divert cargoes into the vacuolar route (Paris and Neuhaus, 2002). It requires only that we postulate the presence within secGFP of a weak vacuolar sorting determinant that redirects a portion of the protein into the PVC, particularly when the rates of synthesis and transport are high or when export from the *trans*-Golgi is impaired. We have not detected classical NTTP or CTTP signals in secGFP, but this does not exclude the existence of vacuolar sorting signals because these are diverse and degenerate in plants (Paris and Neuhaus, 2002). Indeed, in yeast, GFP is sorted with high efficiency to the vacuole via a pathway mediated by the Vps10 receptor (Kunze et al., 1999; Humair et al., 2001). In this respect, it is notable that the fluorescence intensity of the secGFP-labeled PVC compartment is often significantly higher than the ER network or Golgi apparatus. It seems unlikely that GFP fluorescence is enhanced in the environment of the PVC relative to the Golgi. In fact, we suspect the PVC has a lower pH than the ER or Golgi because we detect little fluorescence in this compartment from secYFP (see Supplemental Movie 6 online), which is a spectral variant of secGFP with a lower pK (Llopis et al., 1998). It appears therefore that secGFP is concentrated in these compartments. This implies a signal-mediated mechanism either to selectively concentrate secGFP, to selectively remove membrane during formation of the PVC, or both. Thus, a weak vacuolar sorting signal coupled with a maturation process similar to those known for other PVC/endosomal pathways (Paris and Neuhaus, 2002; Jurgens, 2004) could account for the appearance of bright secGFP-labeled PVC compartments. Consistent with this hypothesis, Ueda et al. (2004) have recently shown that the proportion of tagged RAB-F1 (ARA6) and RAB-F2 (RHA1 and ARA7) proteins on the PVC in Arabidopsis protoplasts is continuously variable, and they have proposed that compartments labeled by one Rab subclass may mature into the other. The diversity of PVC/endosomal compartments may account for the differing relative fluorescence of secGFP and YFP-RAB-F2^{b} in individual PVCs. Furthermore, although YFP-RAB-F2^{b} is localized to the PVC (Kotzer et al., 2004; Lee et al., 2004), a proportion was found to associate with Golgi stacks in this system (Kotzer et al., 2004).

Our observations do not exclude the possibility that RAB-E1^{d}[NI] inhibits retrograde transport of secGFP from the PVC to the Golgi, which could also give rise to bright secGFP-labeled PVC. However, we do not favor this possibility because it seems likely that retrograde and anterograde traffic would be coupled, which would result in impairment of traffic to the vacuole. By contrast, however, we observed that trafficking of secGFP and aleu-GFP to the vacuole continued and was often enhanced in the presence of RAB-E1^{d}[NI].

Our observations with secRFP also make it unlikely that the PVC is labeled by secGFP as a result of fluid-phase endocytosis after exocytosis. This possibility is plausible owing to circumstantial evidence that places the RAB-F2^{b}-labeled PVC in the endocytic pathway as well as the vacuolar pathway: the RAB-F2^{b}-labeled PVCs are labeled by FM4-64 in tobacco (this report) and Arabidopsis (Ueda et al., 2001), their morphology is altered in the *gnom* mutant that is defective in endocytic recycling (Geldner et al., 2003), and they colocalize with fusions to vacuolar sorting receptors that have recently been localized to multivesicular bodies (Kotzer et al., 2004; Tse et al., 2004), which receive endocytosed materials in plant and animal cells (Raiborg et al., 2003; Jurgens, 2004; Tse et al., 2004). However, secRFP fluorescence is stronger than that of secGFP in the environment of the cell wall (this report) and the vacuole (M. Samalaova, J. Legen, and I. Moore, unpublished data), so if secGFP labeled the PVC after fluid-phase endocytosis from the cell wall, we would expect to see secRFP fluorescence in the same endocytic compartments, but we did not.

In contrast with YFP-RAB-E1^{d}, which precisely colocalized with Golgi stacks, YFP-RAB-D2^{a} exhibited a less systematic and complete association. Although YFP-RAB-D2^{a}–labeled punctate structures were often clearly associated with the Golgi stacks and moved together with them, colocalization was not precise, and morphologically similar structures were regularly observed in isolation from the stacks. Similar behavior was reported recently for a YFP-tagged Sar1 protein, which was shown by fluorescence recovery after photobleaching analysis to cycle rapidly on and off these Golgi-associated structures (daSilva et al., 2004). It was proposed that the Sar1-labeled structures represented mobile ER export sites at which COPII vesicles form. Given the role of RAB-D2^{a} in ER–Golgi traffic (Batoko et al., 2000; Saint-Jore et al., 2002), the same may be true for the YFP-RAB-D2^{a}–labeled structures.

The Rab-E subclass is apparently orthologous to Sec4p and Ypt2 that are required for traffic from the Golgi to PM in *S. cerevisiae* and *S. pombe*, respectively (Salminen and Novick, 1987; Haubruck et al., 1990; Craighead et al., 1993; Guo et al., 1999). The most similar mammalian subclasses are the paralogous Rab8, Rab10, and Rab13 subclasses that are implicated in transport to the PM and tight junctions (Huber et al., 1993; Zerial and McBride, 2001), but mammalian cells have elaborated other Rab subclasses in this branch of the pathway, and these have a variety of trafficking functions that are often specific to mammalian cells (Zerial and McBride, 2001; Rutherford and Moore, 2002). Although Arabidopsis has five loci in the Rab-E branch, their high degree of sequence similarity suggests that they belong to a single subclass. Furthermore, we found that a second member of the family, RAB-E1^{c} (ARA3), also targets YFP to the Golgi apparatus via a saturable nucleotide-dependent mechanism (L. Camacho and I. Moore, unpublished data). Thus, it appears that the radiation of Rab functions that characterizes

this branch of the mammalian Rab family has not occurred in plants. Although it is possible that individual plant Rab-E loci may function in particular developmental or physiological contexts (Fleming et al., 1993; Bogdanove and Martin, 2000; Hauck et al., 2003; Moshkov et al., 2003; Hwang and Gelvin, 2004), insertion mutants in Arabidopsis Rab-E loci have yet to reveal an informative membrane trafficking phenotype (S. Rutherford and I. Moore, unpublished data). It is possible that in the higher plant lineage, versatility in post-Golgi trafficking has evolved through diversification of other subclasses, such as the extremely large Rab-A subclass (Rutherford and Moore, 2002).

METHODS

Molecular Cloning and Generation of AtRAB-E1^d[NI] and Various Marker Proteins

Standard molecular techniques were followed as described by Ausubel et al. (1999). The generation of plasmids pVKH-secGFP, pVKH-ST-GFP, pVKH-GFP-HDEL, and RAB-D2^a[NI] is described by Batoko et al. (2000). YFP-RAB-F2^b is described by Kotzer et al. (2004). pVKH-N-ST-YFP is described by Brandizzi et al. (2002b). pVKH-YFP-HDEL was a gift of F. Brandizzi and C. Hawes (Oxford Brookes University, Oxford, UK). The RAB-E1^d coding region was amplified from a cDNA clone using primers PAR8-1 and PAR8-4 (PAR8-1, 5′-AATGGATCCGCTCGAGCACCATGGCGGTTGCGCCGGC-3′; PAR8-4, 5′-TAGCGGGATCCCTAAACGTAACTACAGCAAGC-3′). The N128I substitution was effected by overlapping PCR using PAR8-1 and PAR8-4 together with PAR8-2 (5′-TTTGATTCCAACCAATATTTT**GTTAAC**ATTATCTGAGG-3′) and PAR8-3 (5′-**GTTAAC**AAAATATTGGTTGGAATCAAAGCTGATATGGA-3′), which created a *Hpa*I site (shown in bold) by silent substitution. The coding sequences of RAB-E1^d and RAB-E1^d[NI] were obtained by digestion with *Xho*I and *Bam*HI (underlined in sequence of PAR8-1 and PAR8-4, respectively) and cloned between the *Sal*I and *Bam*HI sites of pVKHEn6-Ara5mΔGUS, a derivative of pVKHEn6-GUS (Batoko et al., 2000). pVKHEn6-Ara5mΔGUS was generated as follows: the RAB-D2^a[NI] coding sequence (Batoko et al., 2000) was cloned as an *Xho*I-*Bam*HI fragment in the corresponding sites of pU-BOP (Samalova et al., 2005); an *Nhe*I-*Bam*HI fragment was isolated and inserted into pVKHEn6-GUS at the *Xba*I and *Bam*HI sites upstream of *uid*A; the *uid*A coding sequence was removed by digestion with *Ecl*136II and *Bam*HI, treatment with Klenow fragment of DNA polymerase I, and religation to regenerate the *Bam*HI site and produce pVKHEn6-Ara5mΔGUS.

To generate the plasmid pVKH18-spo:GFP, the *Xba*I-*Sac*I fragment of spo:GFP in the plasmid pUC18-spo:GFP (Sohn et al., 2003) (kindly provided by Inhwan Hwang [Pohang University of Science and Technology, Pohang, Korea]) was excised and used to replace the GUS coding sequence in the plasmid pVKHEn6-GUS (Batoko et al., 2000).

YFP-Rab fusions were generated with an HA epitope–tagged version of the Venus variant of enhanced YFP (Nagai et al., 2002) in vector pVKHEn6-HAvenus. This was constructed by amplification of the Venus coding sequence using 5′-HA-YFP (5′-AATATCTAGATACCATGTATCCATACGATGTTCCAGATTATGCTGTGAGCAAGGGCGACGAG-3′) and 3′-HA-YFP (5′-ATTAGGATCCTTAT**GTCGAC**TCACTAGTCTTTGACAGCTCGTCCATG-3′) and cloning the product between the *Xba*I and *Bam*HI sites of pVKHEn6-ST-GFP (Saint-Jore et al., 2002). Wild-type and mutant AtRAB-D2^a (Batoko et al., 2000) and AtRAB-E1^d sequences were isolated as *Xho*I-*Bam*HI fragments and inserted between the *Sal*I (bold) and *Bam*HI sites of pVKHEn6-HAvenus. The S22N substitution was introduced into the AtRAB-D2^a (ARA5, AtRab1b) cDNA by overlapping PCR using PAR1 and PAR2 (Batoko et al., 2000) and A5S22N-5′ (5′-CTGGCGTAGGCAAGAATTGTCTACTTTTGAGATTC-3′) and A5S22N-3′ (5′-GAATCTCAAAAGTAGACAATTCTTGCCTACGCCAG-3′), which also introduced an additional *Acc*I site (underlined) by silent mutagenesis. Similarly, the S29N substitution was introduced into the RAB-E1^d cDNA by overlapping PCR that also introduced an additional *Acc*I site by silent mutagenesis adjacent to the S29N substitution (the sequence 5′-AGTTGTTTGTTA-3′ encoding SCLL was changed to 5′-AATTGTCTACTA-3′ encoding NCLL). The RAB-E1^{d}ΔCC clone was generated by PCR using PAR8-1 and RabE1.d-ΔCC-*Bam*HI-R (5′-TTTGGATCCCTAAACGTAACTAGCTGACTTCTC-3′, which lacks the sequence encoding for the two C-terminal Cys residues). pVKHEn6-secRFP was generated by isolating the mRFP1 (Campbell et al., 2002) coding sequence from ST-RFP (a gift of F. Brandizzi [University of Saskatchewan, Saskatoon, Canada]) using *Sal*I and *Sac*I and cloning it between the corresponding sites of pVKH-N-secGFP (Batoko et al., 2000), replacing the glycosylated GFP with mRFP1 downstream of the signal sequence.

Transient Expression in Tobacco Epidermal Cells

Transient expression or coexpression of Rab constructs and fluorescent markers in tobacco (*Nicotiana tabacum*) leaf lower epidermal cells was performed according to Batoko et al. (2000), except that plants were cultivated in constant light unless otherwise stated. Unless otherwise stated, the bacterial OD_{600} used for infiltration of the lower epidermis was 0.05 for untagged RAB-E1^d wild type and mutant, 0.03 for RAB-D2^a[NI], and 0.01 for GFP/YFP/RFP constructs.

E64-d Treatment and FM4-64 Staining

Thirty-three to 36 h after infiltration with *Agrobacterium tumefaciens*, shortly after the onset of secGFP accumulation, infected areas of the leaf were infiltrated with 400 μM E64-d (stock solution 200 mM in dimethylsulfoxide; Bachem, St. Helens, UK). The E64-d–infiltrated leaves were excised from the plant and floated on a solution of 200 μM E64-d at 20°C in darkness. Cells were imaged ~14 h later, when steady state secGFP accumulation and transport was at its maximum. FM4-64 staining of cells coexpressing secGFP and RAB-E1^d[NI] was performed by submerging pieces (~5 mm^2) of transfected leaves in 8.2 μM FM4-64 (stock solution 8.2 mM in water; Molecular Probes, Leiden, The Netherlands) for 30 to 60 min. Quantitative estimates of the degree of vacuolar fluorescence in medial optical sections through epidermal cells were made using the histogram function of the Zeiss LSM software version 2.8 (Jena, Germany) to determine the average pixel intensity in regions of interest defined within the vacuoles. The average pixel intensity in uninfected cells was used to determine the background signal, which was subtracted from each datum. Depending on the transfection efficiency and the magnification at which images were acquired in each of the four quantified experiments, the brightest 5 to 15 cells in each image were quantified. Unusually small cells with low vacuolar volumes were excluded from the analysis because these tended to show very high vacuolar fluorescence relative to other cells in all samples. In each experiment, the average vacuolar fluorescence in each sample was normalized to the value calculated for secGFP + E64-d.

Sampling and Confocal Analyses

Unless otherwise stated, 65 to 72 h after infiltration of leaves with Agrobacterium strains, lower epidermis was analyzed with an upright Zeiss LSM 510 laser scanning microscope, using a 10× objective for low magnification imaging and either a C-apochromat 40×/1.2NA water-immersion or a Plan-apochromat 63×/1.4NA oil-immersion lens for higher magnification images. Pieces of leaf were sampled randomly from the infected area and mounted in water for simple observation or in a 0.05% aqueous solution of the nonfluorescent surfactant Pluronic F-127 (Molecular Probes) for quantitative imaging of secGFP. For single

GFP fluorescence analyses (Figures 1, 2, 5, and 6), we used the 488-nm excitation line of a 25-mW argon ion laser and a 505- to 530-nm band-pass filter in the single-track facility of the microscope. To quantify relative GFP fluorescence intensity, a Plan-Neofluor 10×/0.3NA lens was used at 1× scan zoom. Detector gain was set to avoid saturated pixels in images of GFP-HDEL expressing leaf epidermis, and detector offset was set to avoid pixels of zero value in the images of uninfected leaf epidermis. Data was acquired in 12-bit depth. The average GFP fluorescence intensity was calculated from at least nine images of each leaf sample, and the experiment was repeated four times. In each experiment, the data were normalized to the average intensity of the sample expressing secGFP and RAB-D2^{a}[NI], standard errors of the means were then calculated, and to correct for background fluorescence, the average value for samples expressing secGFP alone was subtracted. For GFP and YFP colocalization experiments, GFP and YFP fluorescence were analyzed using the 458- and 514-nm excitation lines from a 25-mW argon laser with the line-sequential multitrack scanning mode of the Zeiss LSM510 microscope. Fluorescence was detected using a 458/514-nm primary dichroic, a 515-nm secondary dichroic, and a 475- to 525-nm band-pass filter for GFP and a 535- to 590-nm band-pass filter for YFP. To detect secGFP together with secRFP or FM4-64, a line-sequential multitrack configuration with 488-nm excitation and a 505- to 530-nm emission filter for GFP and 543-nm excitation from a He-Ne laser and a 585- to 615-nm emission filter for either secRFP or FM4-64 fluorescence were used. Images were processed with LSM 2.8 or 3.2 (Zeiss) and Photoshop 5.0 (Adobe Systems, San Jose, CA) software.

ACKNOWLEDGMENTS

We thank Inhwan Hwang (Pohang University of Science and Technology, Pohang, Korea) for providing plasmid pUC18-spo:GFP, Amanda Kotzer and Chris Hawes (Oxford Brookes University, Oxford, UK) for providing YFP-RAB-F2^{b} and Arabidopsis RAB-F2^{b}[SN], Jean-Marc Neuhaus (University of Neuchatel, Switzerland) for aleu-GFP, Roger Tsien (Howard Hughes Medical Institute, University of California, San Diego, CA) for mRFP1, and Federica Brandizzi (University of Saskatchewan) for a plasmid expressing ST-RFP. We also thank Marketa Samalova (University of Oxford, Oxford, UK) for assistance with subcloning and Mark Fricker and Hazel Betts (University of Oxford) for discussions and advice on quantitative imaging. H.B. is a research associate of the Belgian fund for scientific research. This work was supported by a grant to I.M. from the Biotechnology and Biological Sciences Research Council.

Received January 24, 2005; revised April 17, 2005; accepted May 9, 2005; published June 21, 2005.

REFERENCES

Arabidopsis Genome Initiative (2000). Analysis of the genome sequence of the flowering plant *Arabidopsis thaliana*. Nature **408,** 796–815.

Ausubel, F., Brent, R., Kingston, R.E., Moore, J.G., Seidman, J.G., Smith, J.A., and Struhl, J.G. (1999). Current Protocols in Molecular Biology. (New York: John Wiley & Sons).

Batoko, H., Zheng, H.Q., Hawes, C., and Moore, I. (2000). A Rab1 GTPase is required for transport between the endoplasmic reticulum and Golgi apparatus and for normal Golgi movement in plants. Plant Cell **12,** 2201–2218.

Boevink, P., Martin, B., Oparka, K., Cruz, S.S., and Hawes, C. (1999). Transport of virally expressed green fluorescent protein through the secretory pathway in tobacco leaves is inhibited by cold shock and brefeldin A. Planta **208,** 392–400.

Boevink, P., Oparka, K., Santa Cruz, S., Martin, B., Betteridge, A., and Hawes, C. (1998). Stacks on tracks: The plant Golgi apparatus traffics on an actin/ER network. Plant J. **15,** 441–447.

Bogdanove, A.J., and Martin, G.B. (2000). AvrPto-dependent Pto-interacting proteins and AvrPto-interacting proteins in tomato. Proc. Natl. Acad. Sci. USA **97,** 8836–8840.

Bolte, S., Brown, S., and Satiat-Jeurnemaitre, B. (2004). The N-myristolylated Rab-GTPase m-Rab$_{mc}$ is involved in post-Golgi trafficking events to the lytic vacuole in plant cells. J. Cell Sci. **117,** 943–954.

Bourne, H.R., Sanders, D.A., and McCormick, F. (1991). The GTPase superfamily: Conserved structure and molecular mechanism. Nature **349,** 117–127.

Brandizzi, F., Fricker, M., and Hawes, C. (2002a). A greener world: The revolution in plant bioimaging. Nat. Rev. Mol. Cell Biol. **3,** 520–530.

Brandizzi, F., Snapp, E.L., Roberts, A.G., Lippincott-Schwartz, J., and Hawes, C. (2002b). Membrane protein transport between the endoplasmic reticulum and the Golgi in tobacco leaves is energy dependent but cytoskeleton independent: Evidence from selective photobleaching. Plant Cell **14,** 1293–1309.

Bucci, C., Parton, R.G., Mather, I.H., Stunnenberg, H., Simons, K., Hoflack, B., and Zerial, M. (1992). The small GTPase rab5 functions as a regulator in the early endocytic pathway. Cell **70,** 715–728.

Campbell, R.E., Tour, O., Palmer, A.E., Steinbach, P.A., Baird, G.S., Zacharias, D.A., and Tsien, R.Y. (2002). A monomeric red fluorescent protein. Proc. Natl. Acad. Sci. USA **99,** 7877–7882.

Cheung, A.Y., Chen, C.Y., Glaven, R.H., de Graaf, B.H., Vidali, L., Hepler, P.K., and Wu, H.M. (2002). Rab2 GTPase regulates vesicle trafficking between the endoplasmic reticulum and the Golgi bodies and is important to pollen tube growth. Plant Cell **14,** 945–962.

Craighead, M.W., Bowden, S., Watson, R., and Armstrong, J. (1993). Function of the ypt2 gene in the exocytic pathway of *Schizosaccharomyces pombe*. Mol. Biol. Cell **4,** 1069–1076.

Crofts, A.J., Leborgne-Castel, N., Hillmer, S., Robinson, D.G., Phillipson, B., Carlsson, L.E., Ashdord, D.A., and Denecke, J. (1999). Saturation of the endoplasmic reticulum retention machinery reveals anterograde bulk flow. Plant Cell **11,** 2233–2247.

daSilva, L.L.P., Snapp, E.L., Denecke, J., Lippincott-Schwartz, L., Hawes, C., and Brandizzi, F. (2004). Endoplasmic reticulum export sites and Golgi bodies behave as single mobile secretory units in plant cells. Plant Cell **16,** 1753–1771.

Denecke, J., De Rycke, R., and Botterman, J. (1992). Plant and mammalian sorting signals for protein retention in the endoplasmic reticulum contain a conserved epitope. EMBO J. **11,** 2345–2355.

Fleming, A.J., Mandel, T., Roth, I., and Kuhlemeier, C. (1993). The patterns of gene expression in the tomato shoot apical meristem. Plant Cell **5,** 297–309.

Geelen, D., Leyman, B., Batoko, H., Di Sansebastiano, G.P., Moore, I., and Blatt, M.R. (2002). The abscisic acid-related SNARE homolog NtSyr1 contributes to secretion and growth: Evidence from competition with its cytosolic domain. Plant Cell **14,** 387–406.

Geldner, N., Anders, N., Wolters, H., Keicher, J., Kornberger, W., Muller, P., Delbarre, A., Ueda, T., Nakano, A., and Jurgens, G. (2003). The Arabidopsis GNOM ARF-GEF mediates endosomal recycling, auxin transport, and auxin-dependent plant growth. Cell **112,** 219–230.

Guo, W., Roth, D., Walch-Solimena, C., and Novick, P. (1999). The exocyst is an effector for Sec4p, targeting secretory vesicles to sites of exocytosis. EMBO J. **18,** 1071–1080.

Gurunathan, S., David, D., and Gerst, J.E. (2002). Dynamin and clathrin are required for the biogenesis of a distinct class of secretory vesicles in yeast. EMBO J. **21,** 602–614.

Harsay, E., and Bretscher, A. (1995). Parallel secretory pathways to the cell surface in yeast. J. Cell Biol. **131,** 297–310.

Harsay, E., and Schekman, R. (2002). A subset of yeast vacuolar protein sorting mutants is blocked in one branch of the exocytic pathway. J. Cell Biol. **156,** 271–285.

Haubruck, H., Engelke, U., Mertins, P., and Gallwitz, D. (1990). Structural and functional analysis of ypt2, an essential ras-related gene in the fission yeast *Schizosaccharomyces pombe* encoding a Sec4 protein homologue. EMBO J. **9,** 1957–1962.

Hauck, P., Thilmony, R., and He, S.Y. (2003). A *Pseudomonas syringae* type III effector suppresses cell wall-based extracellular defense in susceptible *Arabidopsis* plants. Proc. Natl. Acad. Sci. USA **100,** 8577–8582.

Huber, L.A., Pimplikar, S., Parton, R.G., Virta, H., Zerial, M., and Simons, K. (1993). Rab8, a small GTPase involved in vesicular traffic between the TGN and the basolateral plasma membrane. J. Cell Biol. **123,** 35–45.

Humair, D., Hernández Felipe, D., Neuhaus, J.M., and Paris, N. (2001). Demonstration in yeast of the function of BP-80, a putative plant vacuolar sorting receptor. Plant Cell **13,** 781–792.

Hwang, H.H., and Gelvin, S.B. (2004). Plant proteins that interact with VirB2, the *Agrobacterium tumefaciens* pilin protein, mediate plant transformation. Plant Cell **16,** 3148–3167.

Jurgens, G. (2004). Membrane trafficking in plants. Annu. Rev. Cell Dev. Biol. **20,** 481–504.

Kotzer, A.M., Brandizzi, F., Neumann, U., Paris, N., Moore, I., and Hawes, C. (2004). AtRabF2b (Ara7) acts on the vacuolar trafficking pathway in tobacco leaf epidermal cells. J. Cell Sci. **117,** 6377–6389.

Kunze, I.I., Hensel, G., Adler, K., Bernard, J., Neubohn, B., Nilsson, C., Stoltenburg, R., Kohlwein, S.D., and Kunze, G. (1999). The green fluorescent protein targets secretory proteins to the yeast vacuole. Biochim. Biophys. Acta **1410,** 287–298.

Lee, G.-J., Sohn, E.J., Lee, M.H., and Hwang, I. (2004). The Arabidopsis Rab5 homologs Rha1 and Ara7 localize to the prevacuolar compartment. Plant Cell Physiol. **45,** 1211–1220.

Leyman, B., Geelen, D., and Blatt, M.R. (2000). Localization and control of expression of Nt-Syr1, a tobacco SNARE protein. Plant J. **24,** 369–381.

Llopis, J., McCaffery, J.M., Miyawaki, A., Farquhar, M.G., and Tsien, R.Y. (1998). Measurement of cytosolic, mitochondrial, and Golgi pH in single living cells with green fluorescent proteins. Proc. Natl. Acad. Sci. USA **95,** 6803–6808.

Moore, I., Schell, J., and Palme, K. (1995). Subclass-specific sequence motifs identified in Rab GTPases. Trends Biochem. Sci. **20,** 10–12.

Moshkov, I.E., Mur, L.A.J., Novikova, G.V., Smith, A.R., and Hall, M.A. (2003). Ethylene regulates monomeric GTP-binding protein gene expression and activity in Arabidopsis. Plant Physiol. **131,** 1705–1717.

Nagai, T., Ibata, K., Park, E.S., Kubota, M., Mikoshiba, K., and Miyawaki, A. (2002). A variant of yellow fluorescent protein with fast and efficient maturation for cell-biological applications. Nat. Biotechnol. **20,** 87–90.

Paris, N., and Neuhaus, J.M. (2002). BP-80 as a vacuolar sorting receptor. Plant Mol. Biol. **50,** 903–914.

Pereira-Leal, J.B., and Seabra, M.C. (2000). The mammalian Rab family of small GTPases: Definition of family and subfamily sequence motifs suggests a mechanism for functional specificity in the Ras superfamily. J. Mol. Biol. **301,** 1077–1087.

Pereira-Leal, J.B., and Seabra, M.C. (2001). Evolution of the Rab family of small GTP-binding proteins. J. Mol. Biol. **313,** 889–901.

Phillips, D.G., Preshaw, C., and Steer, M.W. (1988). Dictyosome vesicle production and plasma membrane turnover in auxin-stimulated outer epidermal cells of coleoptile segments from *Avena sativa* (L.). Protoplasma **145,** 59–65.

Raiborg, C., Rusten, T.E., and Stenmark, H. (2003). Protein sorting into multivesicular endosomes. Curr. Opin. Cell Biol. **15,** 446–455.

Rutherford, S., and Moore, I. (2002). The Arabidopsis Rab GTPase family: Another enigma variation. Curr. Opin. Plant Biol. **5,** 518–528.

Saint-Jore, C.M., Evins, J., Batoko, H., Brandizzi, F., Moore, I., and Hawes, C. (2002). Redistribution of membrane proteins between the Golgi apparatus and endoplasmic reticulum in plants is reversible and not dependent on cytoskeletal networks. Plant J. **29,** 661–678.

Salminen, A., and Novick, P.J. (1987). A ras-like protein is required for a post-Golgi event in yeast secretion. Cell **49,** 527–538.

Samalova, M., Brzobohaty, B., and Moore, I. (2005). pOp6/LhGR: A stringently regulated and highly responsive dexamethasone-inducible gene expression system for tobacco. Plant J. **41,** 919–935.

Schmitt, H.D., Wagner, P., Pfaff, E., and Gallwitz, D. (1986). The *ras*-related YPT1 gene product in yeast: A GTP-binding protein that might be involved in microtubule organization. Cell **47,** 401–412.

Seabra, M.C., and Wasmeier, C. (2004). Controlling the location and activation of Rab GTPases. Curr. Opin. Cell Biol. **16,** 451–457.

Segev, N. (2001). Ypt and Rab GTPases: Insight into functions through novel interactions. Curr. Opin. Cell Biol. **13,** 500–511.

Sohn, E.J., Kim, E.S., Zhao, M., Kim, S.J., Kim, H., Kim, Y.W., Lee, Y.J., Hillmer, S., Sohn, U., Jiang, L., and Hwang, I. (2003). Rha1, an Arabidopsis Rab5 Homolog, plays a critical role in the vacuolar trafficking of soluble cargo proteins. Plant Cell **15,** 1057–1070.

Surpin, M., and Raikhel, N. (2004). Traffic jams affect plant development and signal transduction. Nat. Rev. Mol. Cell Biol. **5,** 100–109.

Takeuchi, M., Ueda, T., Sato, K., Abe, H., Nagata, T., and Nakano, A. (2000). A dominant negative mutant of Sar1p GTPase inhibits protein transport from the endoplasmic reticulum to the Golgi apparatus in tobacco and Arabidopsis cultured cells. Plant J. **23,** 517–525.

Tamura, K., Shimada, T., Ono, E., Tanaka, Y., Nagatani, A., Higashi, S.I., Watanabe, M., Nishimura, M., and Hara-Nishimura, I. (2003). Why green fluorescent fusion proteins have not been observed in the vacuoles of higher plants. Plant J. **35,** 545–555.

Tamura, K., Yamada, K., Shimada, T., and Hara-Nishimura, I. (2004). Endoplasmic reticulum-resident proteins are constitutively transported to vacuoles for degradation. Plant J. **39,** 393–402.

Thiel, G., Kreft, M., and Zorec, R. (1998). Unitary exocytotic and endocytotic events in *Zea mays* L. coleoptile protoplasts. Plant J. **13,** 117–120.

Tse, Y.C., Mo, B., Hillmer, S., Zhao, M., Lo, S.W., Robinson, D.G., and Jiang, L.W. (2004). Identification of multivesicular bodies as prevacuolar compartments in *Nicotiana tabacum* BY-2 cells. Plant Cell **16,** 672–693.

Ueda, T., Uemura, T., Sato, M.H., and Nakano, A. (2004). Functional differentiation of endosomes in Arabidopsis cells. Plant J. **40,** 783–789.

Ueda, T., Yamaguchi, M., Uchimiya, H., and Nakano, A. (2001). Ara6, a plant-unique novel type Rab GTPase, functions in the endocytic pathway of *Arabidopsis thaliana*. EMBO J. **20,** 4730–4741.

Vernoud, V., Horton, A.C., Yang, Z., and Nielsen, E. (2003). Analysis of the small GTPase gene superfamily of Arabidopsis. Plant Physiol. **131,** 1191–1208.

Walch-Solimena, C., Collins, R.N., and Novick, P.J. (1997). Sec2p mediates nucleotide exchange on Sec4p and is involved in polarized delivery of post-Golgi vesicles. J. Cell Biol. **137,** 1495–1509.

Walworth, N., Goud, B., Kastan Kabcenell, A., and Novick, P.J. (1989). Mutational analysis of *SEC4* suggests a cyclical mechanism for the regulation of vesicular traffic. EMBO J. **8,** 1685–1693.

Zerial, M., and McBride, H. (2001). Rab proteins as membrane organizers. Nat. Rev. Mol. Cell Biol. **2,** 107–117.

Zheng, H., Kunst, L., Hawes, C., and Moore, I. (2004). A GFP-based assay reveals a role for RHD3 in transport between the endoplasmic reticulum and Golgi apparatus. Plant J. **37,** 398–414.